UNIVERSITA' DEGLI STUDI DI MILANO-BICOCCA

Facoltà di Scienze Matematiche, Fisiche e Naturali
Dipartimento di Biotecnologie e Bioscienze
Dottorato di ricerca in Biologia
XXII ciclo

POLYNUCLEOTIDE PHOSPHORYLASE FROM *Escherichia coli*: REGULATION MECHANISMS AND SUBSTRATE BINDING

Dr. Elisa MAZZANTINI

Tutor: Prof. Paolo TORTORA
Cotutor: Prof. Gianni DEHO'

A Benni, a Simo
e ai miei amici

“Se sarete quello che dovete essere,
metterete fuoco in tutta l’Italia.
Non accontentatevi delle piccole cose:
Egli, Iddio, le vuole grandi”
(Santa Caterina da Siena)

Index

ABBREVIATIONS

Abs	absorbance
Amp	ampicillin
BBF	bromophenol blue
Bis-acrilamide	N,N'-metilen-bisacrilamide
bp	base pair
BSA	bovine serum albumine
Caf	chloramphenicol
DTT	dithiotreitol
EDTA	etilendiaminetetraacetic acid
EtBr	etidium bromide
H	hours
Kan	Kanamycin
kDa	chilodalton
IPTG	isopropil-tio-D-galattopiranoside
min	minuts
PAGE	polyacrylamide gel electrophoresis
PBS	phosphate buffer
PMSF	phenilmethansulphonilfluoride
PNPase	polynucleotide phosphorylase
rpm	revolutions per minute
SDS	sodium dodecilsulfate
sec	seconds
TAE	tris-acetate-EDTA buffer
TEMED	N,N,N',N'tetramethylethylendiamine
Tris	tris [hydroxymetil] aminomethane
UV	ultraviolet
wt	wild type

ABSTRACT

Polynucleotide phosphorylase (PNPase), an enzyme conserved in *Bacteria* and eukaryotic organelles, processively catalyzes the phosphorolysis of RNA releasing nucleotide diphosphates and the reverse polymerisation reaction. In *Escherichia coli,* both reactions are implicated in RNA decay, as addition of either polyA or heteropolymeric tails targets RNA to degradation. PNPase may also be associated with the RNA degradosome, a heteromultimeric protein machine that can degrade highly structured RNA. Many issues are still open regarding composition, molecular interactions, assembly pathway, mechanism of action, and physiological significance of this molecular machine. We observed that ATP binds to PNPase and allosterically inhibits both its phosphorolytic and polymerization activities. Our data suggest that PNPase-dependent RNA tailing and degradation occur mainly at low ATP concentrations, whereas other enzymes may play a more significant role at high energy charge. These findings connect RNA turnover with the energy charge of the cell and highlight unforeseen metabolic roles of PNPase.

We also developed investigations aimed at identifying the ATP-binding site of PNPase. By a modeling analysis we tentatively identified residues of two putative ATP-binding sites: Phe77, Phe78, Arg79 in one site; Phe56, Arg93, Phe103 in the other. We replaced by alanine the six residues, but in no case the inhibitory effect was abolished. This indicates that the modeling analysis failed to identify the nucleotide binding site. However, during these studies we also observed that the mutants R79A and F77A displayed reduced polymerization activity using ADP as a substrate, which suggests that the two mutated residues are implicated in the catalytic activity of enzyme.

To check this hypothesis we determined the kinetic parameters for ADP, P_i and polyA of our mutants. In the case of R79A, both K_m values for ADP and phosphate were much larger than in the wild type (wt), whereas in F77A they were very similar to that of wt. Furthrmore, the k_{cat}s of these mutants were of the same order of magnitude of that of the wt. These results suggest that Arg79 but not Phe77 compose the nucleoside diphosphate binding-site.

We also determined the K_m for polyA to check a possible involvement of the two residues in RNA binding, as previously suggested. Nevertheless, we could not demonstrate significant differences compared to that of the wt, which suggests that either these residues do not interact with RNA, or single mutations are not sufficient to cause a significant decrease in RNA binding.

To further characterize the substrate-binding site of PNPase we performed a further modeling analysis using Autodock4. We analyzed *in silico* wt PNPase and the mutant R79A with bound ADP. In the mutant R79A, the affinity between the enzyme and the substrate was smaller than that of the wt. These data confirm that Arg79 is involved in nucleoside diphosphate binding. The computational analysis also points to an involvement of residues Arg80 and Arg83 in ADP binding. We therefore produced the single mutants R80A and R83A and the double mutant R79/80A. None of the single mutants displayed drastic variations in the k_{cat} compared to the wt, which shows that the mutated residues are not directly implicated in the catalytic process. In the single mutants, the K_m for phosphate was much larger than that of the wt, Also R80A displayed a K_m for ADP two order of magnitude larger but, in contrast, R83A had a smaller K_m. In the double mutant, enzyme activity was very low, which prevented us

from performing a reliable determination of the kinetic parameters. The K_m for polyA was not significantly changed by the mutations.

Based on these results it can be concluded that RNA binding is not compromised by the described mutations and that the relevant residues might be instead involved in phosphate and/or ADP terminal phosphate binding. This conclusion is however conflicting with recent reports that point to a role for Arg79 and Arg80 in RNA binding. Thus, it is likely that the overall pattern of interactions involved in substrate binding and catalysis is far more complex than we initially hypothesized. In particular, it is known that PNPase has the additional RNA binding domains KH and S1: thus, the K_m for RNA might not significantly change even though the residues we mutated are actually involved in RNA binding. A better understanding of this issue might be provided either using a shorter RNA substrate, or characterizing a PNPase variant deleted of the KH and S1 domains into which the aforementioned mutations have been introduced, as we are planning to do.

1. INTRODUCTION

1.1 Rna degradation in bacteria

Gene expression is controlled at four major steps: efficiency of transcription, which depends on the control of both transcription initiation and elongation, stability of the transcripts, mRNA translation efficiency, and post-translational activation, including protein targeting. The relevance of each step may vary from gene to gene and according to different physiological conditions. Obviously, the two latter steps only implicate protein-encoding genes .

RNA stability was long recognised as an important step in gene expression. However, only over the past 20 years considerable progress has been made in understanding the molecular details of mRNA decay in both prokaryotes and eukaryotes. In retrospective, these studies seem to have been complicated especially by the redundancy of degradation pathways and the plethora of RNA degrading enzymes that may be implicated in more than one aspect of RNA metabolism, namely i) processing of RNA precursor molecules (especially, but not only, for the maturation of stable RNAs); ii) quality control of stable RNA and mRNA, which eliminates non-functional or even toxic RNA fragments generated by abnormal transcription or maturation events; and iii) *bona fide* mRNA turnover that may be regulated so as to control gene expression .

Prokaryotic mRNAs are usually more unstable than those of eukaryotes, although the decay rates of different mRNA may vary over a wide range, and can change under different physiological conditions. For example, in *Escherichia coli*, mRNA half-lives can range from few seconds to half an hour (Grunberg-Manago, 1999), and during the cold acclimation phase

some cold shock mRNAs may increase their half life from 45 seconds up to 70 minutes (Gualerzi, Giuliodori, and Pon, 2003). Several *cis*-acting elements (secondary structures of 5' or 3' RNA regions) or diffusible factors (ribosomal proteins, ribonucleases, antisense RNAs) may control RNA stability. Moreover, the modulation of *trans*-effector activity and the accessibility of the *cis*-acting regulatory sequences may add, both in prokaryotes and eukaryotes, further levels of complexity to the process (Baker and Condon, 2004).

mRNAs can be degraded by a number of mechanisms that act independently, in parallel or sequentially, and may be modulated by growth conditions, environmental signals, and the efficiency of translation. It is difficult to assess the contribution of each of these elements to mRNA stability. (Petersen, 1991).

Most of what we know of the pathways of messenger RNA (mRNA) degradation in Bacteria comes from studies done in *E. coli*. In this bacterium, mRNA degradation is generally triggered by endonucleolytic cleavages, followed by 3'-to-5' exonucleolytic RNA decay (Fig. 1.1). The principal instigator of this process under balanced growth conditions is the essential ribonuclease RNase E. However, other endonucleases such as its paralogue RNase G, RNase III (which acts specifically on double stranded structures) and RNase P (which primarily maturates tRNA) are implicated. Following an initial endonucleolytic cleavage which often occurs within the coding region thus inactivating translation, additional cleavages break down the mRNA into fragments. Endonucleolytic cleavages generate new unprotected 3'-ends that are rapidly degraded by exonucleases (Condon, 2007).

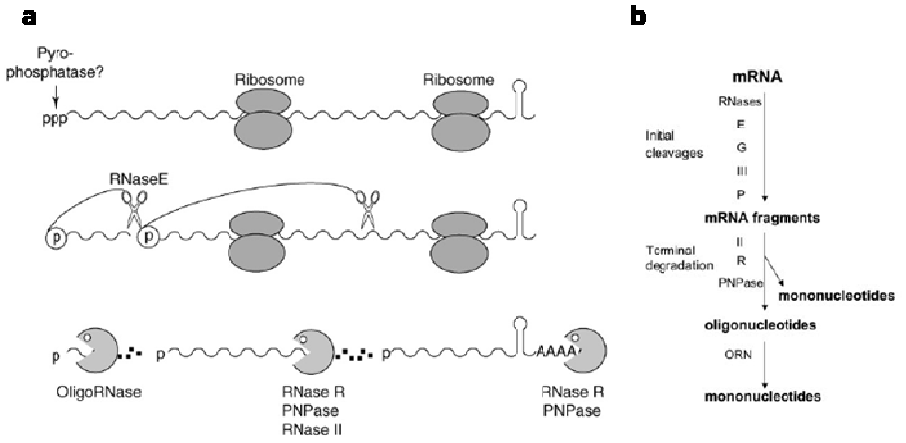

Figure 1.1. (a) Endonucleolytic cleavage of mRNAs by 5'-monophosphate-dependent RNase E is indicated by scissors symbols. 3'-to-5' exonucleolytic degradation of the cleaved intermediates by the major exoribonucleases RNase R, PNPase and RNase II is indicated by the 'Pacman' symbols. Fragments containing RNA structure, such as terminator hairpins, require polyadenylation before being degraded. Small fragments in the 2–5 nt range are degraded by oligoribonuclease. (From Condon, 2007) (b) mRNA degradation in *E. coli*. Initial cleavages during mRNA decay are carried out by the endoribonucleases, RNases E, G, III and P. Terminal degradation of mRNA decay intermediates utilizes the processive exoribonucleases, RNases II, R or PNPase, followed by oligoribonuclease (ORN) to remove 5' terminal oligonucleotides (From Deutscher, 2006).

Three large, processive 3'–5' exoribonucleases are primarily responsible for degradation of mRNA fragments, namely polynucleotide phosphorylase (PNPase), RNase II and RNase R (Deutscher and Li, 2001). These processive exoribonucleases are unable to complete the degradation of mRNA fragments as they are relatively inactive against short oligonucleotides (Deutscher and Li, 2001). These residual products are digested to mononucleotides by oligoribonuclease, an exoribonuclease specific for very short chains (Ghosh and Deutscher, 1999).

Interestingly, RNase E may function both as an independent protein and in a multiprotein machine, the RNA degradosome. This complex contains, in addition, PNPase, the RNA helicase RhlB, and the glycolytic enzyme enolase. The association of an endoribonuclease, an

exoribonuclease and an RNA helicase would seem to make the degradosome ideally suited for the breakdown of RNA molecules.

Although initiated by RNase E internal cleavages, it appears that *E. coli* mRNAs are degraded in a 5' to 3' direction. This may be explained by the properties of RNase E, which is activated by the binding to a monophosphorylated 5'-end and would make sequential endonucleolytic cuts proceeding from the 5' to the 3'-end. How RNase E-dependent degradation of native mRNAs with triphosphorylated 5'-end (thus excepting RNAs previously processed by the RNase III) may be initiated has long been an unsolved problem. The hypothesis that RNase E could cleave at very low efficiency 5'-triphosphorylated RNAs, thus posing a rate-limiting factor to decay initiation, did not find support by RNase E structure (Callaghan et al., 2005).

Recently, Belasco and collaborators (Celesnik et al., 2007) have provided evidence for a pyrophosphatase acting on native mRNAs and more recently the same group identified the *E. coli* protein RppH (formerly NudH/YgdP) as the RNA pyrophosphohydrolase that creates the substrate for RNase E initial cleavage (Deana, Celesnik, and Belasco, 2008). This is reminiscent of the mRNA decapping in eukariotes that targets the transcripts to degradative pathways.

Elements at the 5' and 3' ends of bacterial and phage messages have been implicated in mRNA stabilization. Most prokaryotic mRNAs end in a 3'-terminal stem-loop structure, which serves as a protective barrier against degradation by 3' exoribonucleases (Belasco et al., 1986; Mott et al., 1985; Chen et al., 1988). In contrast, 5’ untranslated region(s) [UTR(s)] can bear regulatory elements that are involved in down- or up-regulation of translation with corresponding effects on mRNA stability.

In general, inefficient ribosome binding to the 5'-ends of canonical mRNAs has been shown to decrease their stability (Wagner and Simons, 1994; Iost and Dreyfus, 1995; Arnold et al., 1998). As mentioned above, the decay of canonical mRNAs is frequently initiated by RNase E cleavages in the 5' UTR of mRNA in A/U-rich regions. Such A/U-rich sequences are frequently found in the vicinity of the ribosome binding site (RBS) of *E. coli* mRNAs. While interacting with the translation initiation region, the 30S ribosome subunit confers protection to a 50-nt region around the start codon (Huttenhofer and Noller, 1994).

Hence, a ribosome bound at the RBS would be anticipated to protect A/U-rich regions flanking the start codon from RNase E cleavage. More reliable information has been obtained by examining the influence of RBS mutations on RNA decay. For example, experiments in *E. coli* have shown that a variety of mRNAs can be significantly destabilized by mutations in the Shine-Dalgarno element that interfere with ribosome binding (Wagner and Simons, 1994; Arnold et al., 1998; Sharp and Bechhofer, 2003). Ribosomal protein S1, which is thought to bind mRNA RBS and favor its association with the ribosome, may play a role in protecting the transcript from RNase E cleavage.

Post-transcriptional mechanisms in bacteria often involve cis- and trans-encoded antisense RNAs (Carpousis, 2003; Majdalani et al., 2005). Most of these small noncoding RNAs (ncRNAs) basepair with the translation initiation region of their target mRNAs, and the resulting inhibition of translation may lead to degradation of the ribosome-free mRNAs by the concerted action of endo- and exoribonucleases.

Another factor only recently implicated in control of bacterial mRNA stability is polyadenylation that promotes exonucleolytic degradation of mRNA (Belasco and Higgins, 1988). It has been shown that secondary

structures at the 3'-end of mRNAs, such as those formed by Rho-independent terminators, impede RNase II and PNPase exonucleolytic, whereas polyadenylation of such ends facilitates their degradation. This has been rationalized by the proposal that polyA tails stimulate mRNA decay by providing a single-stranded extensions to facilitate the action of exonucleases.

1.1.1 Endoribonucleases

In *E. coli*, the principal pathway for mRNA decay begins with cleavage of mRNA at an internal site, followed by degradation of the resulting RNA fragments by a combination of endonuclease and 3'-exonuclease digestion. RNase E (coded by the *rne* gene) is the endoribonuclease thought to initiate degradation of most mRNAs in *E. coli*. RNase E is a 1061-amino acid protein that comprises an amino-terminal catalytic domain, a central arginine-rich region, and a carboxy-terminal domain that functions as a scaffold for assembly of a multiprotein complex known as the RNA degradosome (Ghora and Apirion, 1978; Ono and Kuwano, 1979; Mudd *et al*., 1990; Babitzke and Kushner, 1991; Melefors and von Gabain, 1991; Taraseviciene *et al*., 1991; McDowall and Cohen, 1996; Vanzo *et al*., 1998).

In addition to RNase E, *E. coli* contains a related endonuclease, RNase G (coded by *rng*, previously known as *cafA*), that is homologous to the catalytic domain but lacks the arginine-rich region and carboxyterminal domain of RNase E (McDowall *et al*., 1993; Okada *et al*., 1994). Not surprisingly, these two enzymes share a number of properties, such as a propensity to cleave RNA within single-stranded AU-rich regions and a preference for 5'-monophosphate RNA substrate (Jiang *et al*., 2000; Tock *et al*., 2000). Nonetheless, the biological functions of these two enzymes in *E.*

coli are quite distinct. Indeed, RNase E is essential for *E. coli* cell growth and plays important roles in mRNA degradation and tRNA and rRNA maturation (Ghora and Apirion, 1978; Ono and Kuwano, 1979; Ray and Apirion, 1981; Li and Deutscher, 2002; Ow and Kushner, 2002), whereas RNase G is a non-essential protein whose absence has no discernable effect on the rate of *E. coli* cell growth or on the degradation or maturation of most RNAs. Notable exceptions are *adhE* and *eno* mRNA decay and 16S rRNA processing, which are RNase G-dependent (Wachi *et al*., 1997; Li *et al*., 1999; Wachi *et al*., 1999; Lee *et al*., 2002). One possible explanation for the much more limited role of RNase G in *E. coli* is its lower cellular concentration, less than 3% of RNase E (Lee *et al*., 2002). Thus, RNase E might be the most important of these two related proteins simply because its absence leaves *E. coli* with an inadequate supply of RNase E/G enzyme activity, whereas the absence of the much less abundant RNase G has little impact on total cellular RNase E/G activity. Alternatively, there may be specificity differences between these enzymes that make RNase E essential and relegate RNase G to a minor role in *E. coli* . In principle, these two explanations could be distinguished by determining whether overproduction of RNase G can compensate for the absence of RNase E in *E. coli* by restoring normal RNA processing and decay and thereby allowing cell growth. Previous efforts to address this question have led to contradictory conclusions. Jiang *et al*. (2000) reported that production of terminally tagged RNase G at six-fold the normal concentration of RNase E is insufficient to restore growth of *E. coli* cells that lack RNase E, despite being well tolerated by *E. coli* cells that contain RNase E. In contrast, Lee *et al*. (2002) reported that production of a tagged form of RNase G at twice the normal concentration of RNase E does restore viability of *E. coli* cells that lack RNase E despite failing to reconstitute normal processing of certain RNA substrates of RNase E *in vivo*.

To determine the basis for these disparate observations, Deana and Belasco (2004) have investigated the differences between RNase G and RNase E. They observed that the ability of RNase G to sustain significant *E. coli* cell growth in the absence of RNase E requires the presence of an unnatural extension of several amino acid residues at the amino or carboxyl terminus of RNase G. Overproduction of wild-type RNase G lacking such an extension or of an RNase G variant bearing the wrong extension cannot normally restore viability to RNase E-deficient *E. coli* cells. Studies of a number of different tRNAs suggest that the growth complementation observed for RNase G bearing an amino-terminal extension is not due to an improvement in tRNA processing. These findings demonstrate the critical importance of the protein amino and carboxyl termini for constraining RNase G function and indicate that RNase E is not required for tRNA production in *E. coli.*

1.1.2 Exoribonucleases

Eight 3' to 5' exoribonucleases have been characterized in *E. coli*; namely polynucleotide phosphorylase (PNPase, coded by *pnp*), RNase II (*rnb*), RNase D (*rnd*), RNase BN (*rbn*), RNase T (*rnt*), RNase PH (rph), RNase R (*rnr*) and oligoribonuclease (*orn*).

Exoribonuclease II (RNase II) is a hydrolytic exonuclease that degrades RNA processively in the 3' to 5' direction releasing 5'-nucleotide monophosphates. Its activity is sequence-independent but is blocked by secondary structures in the RNA, and polyA is the preferential substrate for this enzyme (Amblar *et al.,* 2005). In *E. coli* RNase II is responsible for 90% of the exoribonucleolytic activity in crude extract (Deutscher *et al.,* 1991). This enzyme and PNPase (a phosphorolytic enzyme; see below) are the two

main exoribonucleases (Arraiano *et al.*, 2003) and mutants deficient in these enzymes have been critical in the understanding of mRNA decay mechanisms (Viegas *et al.*, 2005).

RNase II expression is differentially regulated at the transcriptional and post-transcriptional levels (Zilhao *et al.*, 1996) and the protein can be regulated by the environmental conditions (Cairrao *et al.*, 2001). *E. coli* RNase II is the prototype of a widespread family of exoribonucleases, and RNase II homologues can be found in prokaryotes and eukaryotes (Mian *et al.*, 1997). In the nucleus and the cytoplasm of eukaryotic cells RNase II is part of the exosome, an essential multiprotein complex of exoribonucleases, involved in processing, turnover and quality control of different types of RNAs (Mitchell *et al.*, 1997). RNase II is often essential for growth (Van Hoof *et al.*, 1999), can be developmentally regulated (Cairrao *et al.*, 2001) and mutations in its gene have been linked with abnormal chloroplast biogenesis (Bollenbach *et al.*, 2005), mitotic control (Noguchi *et al.*, 1996) and cancer (Lim *et al.*, 1997). In prokaryotic cells there is an additional RNase II-like enzyme, RNase R, that has been shown to be required for virulence and to be involved in mRNA degradation and RNA and protein quality control (Cheng *et al.*, 1998; Andrade *et al.*, 2006; Cairrao *et al.*, 2006). All the enzymes included in this family are large polypeptides sharing sequence identity and distinctive conserved motifs, suggesting the presence of functional domains. The N-terminal region is the most variable in both length and sequence among all proteins of the family, but sequence inspection predicts that most of them contains one or more putative RNA binding domains. Sequence homology analysis reveals that the N-terminal region of *E. coli* RNase II contains a sequence similar to the cold shock domain (CSD). This domain has been described as a single-stranded nucleic acid binding domain that functions as a RNA chaperone in bacteria and is

involved in regulating translation in eukaryotes (Graumann *et al.*, 1998). At the C-terminus, the presence of a S1 RNA-binding domain has been proposed for all RNase II family members. This domain was originally identified in ribosomal protein S1 (Boni *et al.*, 1991) and is found in a large number of RNA-associated proteins. In the central region of RNase II protein there is a highly conserved stretch of about 400 amino acids, which contains four prominent sequence motifs (Zuo *et al.*, 2001). This central region spans the so-called RNB domain and has been proposed to be the catalytic domain.

Recently Amblar *et al.* (2006) have showed that the three domains predicted for *E. coli* RNase II are in fact able to act independently and they demonstrated that the RNB putative domain by itself is still able to efficiently bind and degrade RNA, indicating the presence of an additional RNA-binding capability of this domain.

1.2 Polynucleotide phosphorylase

1.2.1 PNPase structure and catalytic activity

PNPase was discovered by Grunberg-Manago and Ochoa while they were studying the mechanism of biological phosphorylation in *Azotobacter vinelandii* (Grunberg-Manago *et al.*, 1955) and was characterized by Littauer and Kornberg (1957) in studies on the nature of ribonucleotide incorporation into nucleic acids in *E. coli*.

PNPase was the first enzyme to be identified that can catalyze the formation of polynucleotides from ribonucleotides. However, unlike the RNA polymerases, PNPase does not require a template and cannot copy one. This enzyme, encoded by *pnp*, catalyzes the reversible reaction of phosphorolysis of polynucleotides, releasing di-phospho nucleosides

(Grunberg-Manago, *et al.*, 1955). This is the main reaction occurring *in vivo* while the di-phospho ribonucleosides polymerization seems to play a secondary role in the poly-adenylation system (Mohanty and Kushner, 2000).

PNPase is expressed in almost all species extending from bacteria to plants and mammals, with the exception of yeast in which it has not been detected (Leszczyniecka *et al.*, 2004). The *pnp* gene is dispensable for *E. coli* growth at 37°C, whereas it is essential at low (below about 18°C) temperatures (Luttinger *et al.*, 1996; Piazza *et al.*, 1996). It is located at 71 min on the *E. coli* map (Berlyn, 1998) together with other cold-shock induced genes such as *nusA*, coding for a trascription elongation factor, *infB,* coding for IF2, and *rbfA*, which is essential at low temperatures (Jones *et al.*, 1996).

The *pnp* gene is located immediately downstream of *rpsO*, which codes for the ribosomal protein S15, and is followed by *nlpI*, coding for a lipoprotein, and *deaD,* coding for a DEAD-box RNA elicase (Jones *et al.*, 1996). Transcription of *pnp* can originate from two different promoters, *rpsOp* (also referred to as P1), upstream of *rpsO*, and *pnp-p* (P2), located between *rpsO* and *pnp* (Portier and Régnier, 1984). Both *pnp* primary transcripts are processed by RNase III (Régnier and Grunberg-Manago, 1990; Robert-Le Meur and Portier, 1992; Jarrige *et al.*, 2001). This originates a mono-cistronic mRNA 2.25 kb long that extends from the RNase III cleavage site to the downstream transcription termination site (Portier *et al.*, 1987).

Bacterial PNPases are homotrimers, each monomer containing two N-terminal RNase PH domains linked by an α-helix domain, and a C-terminal RNA-binding S1 and KH domain. The crystal structure of *Streptomyces antibioticus* PNPase has been determined ten years ago, revealing a

doughnut-shaped structure, formed by six RNase PH domains in a homotrimer (Symmons *et al.* 2000). This overall organization of a hexameric ring structure with the RNA-binding domain associated on the top of the ring is similar to those of archeal (Buttner *et al.* 2005; Lorentzen *et al.* 2005) and human exosome (Liu *et al.* 2006). Core complexes indicate evolutionary links in structure and function between PNPase and exosome in RNA degradation (Symmons *et al.* 2002; Lin-Chao *et al.* 2007).

Recently, wild type (wt) *E. coli* PNPase and KH/S1-truncated mutant have been crystallized, alone or in association with different substrates (Shi *et al.* 2008; Nurmohamed *et al. 2009).* The structures were solved by molecular replacement using the crystal structure of *S. antibioticus* PNPase (PDB accession code 1E3P), that share 47% sequence identity based on structure alignment, as the searching model. The final model of the full length PNPase crystal structure contains two RNAse PH domains and one α-helical linker domain from residues 17 to 565 (Fig. 1.2).

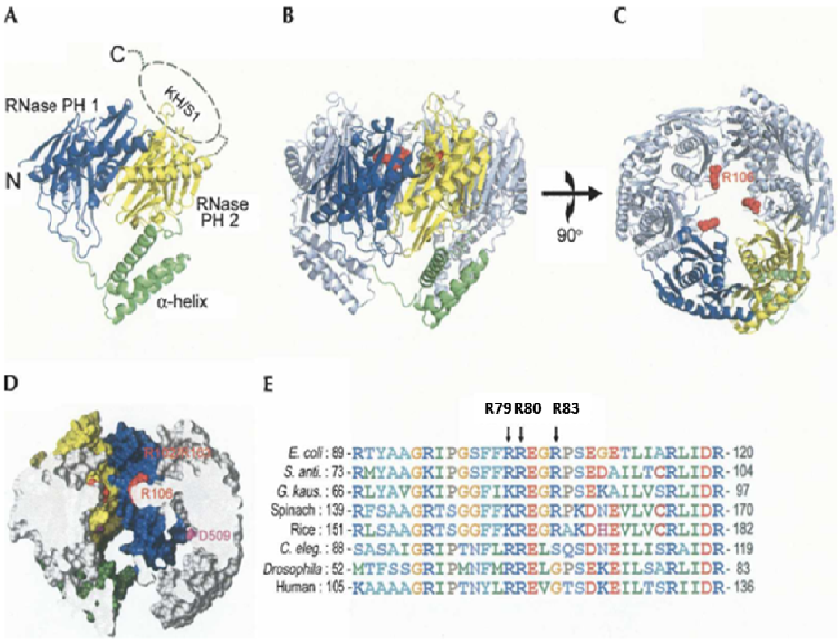

Figure 1.2. Crystal structure of *E. coli* PNPase. A) The structure of a monomeric PNPase contains three domains: the RNase PH1 domain (blue), the α-helix linker domain (green), and the RNase PH2 domain (yellow). The C-terminal KH/S1 domain (marked by dashed circle) is disordered and thus is not visible in the crystal structure. B) The side view of the trimeric PNPase with the only one of the monomers colored in blue, yellow, and green. The other two monomers are colored in gray. The side chain of R83A is displayed as a red sphere model. C) The top view of the trimeric PNPase. The homotrimeric PNPase is assembled into a ring-like structure with a central channel. D) The side view of the halved PNPase trimer shows the shape of the hollow central channel. The molecular surface of RNase PH1 domain is displayed in yellow, whereas the surface of RNase PH2 domain is displayed in blue. The channel has two constricted necks formed by arginine residues in the first RNase PH domain, Arg79 and Arg80 in the upper neck closer to the channel entrance, and Arg83 in the lower neck closer to the active site. E) Sequence alignment of PNPase from different species shows that the basic arginine residues, Arg79, Arg80 and Arg83 are higly conserved in bacteria, plants and animals. The alignment was generated by ClustalW (http://www.ch.embnet.org/software/ClustalW.html) (from Shi et al. 2008).

The C-terminal KH and S1 domains are not visible. Likely, these domains are disordered as a whole in the crystal structure since they are connected to the second RNase PH domain by a long flexible loop. Superposition of *E. coli* PNPase to that of *S. antibioticus* gave an RMSD of 1.45 Å over 443 C_α atoms, suggesting that the two bacterial structures are highly similar.

As expected, the homotrimer of PNPase forms a ring-like structure containing a central channel. The halved trimeric PNPase shows that the central channel contains two constricted necks with three arginine residues located in the neck regions: Arg79 and Arg80 in the upper neck closer to the channel entrance, and Arg83 in the lower neck closer to the active site located in the second RNase PH domain. Arg 79 and Arg 80 are part of the conserved FFRR loop. Both RNase PH domains, PH1 and PH2, contribute to the channel surface inside of the PNPase (Fig. 2D) (Shi *et al.* 2008). The structure of PNPase core in complex with modified RNA shows that Phe77 (the first residue of FFRR loop) of each PNPase core monomers makes an aromatic stacking contact with an RNA base.

Crystallographic results show that FFRR loop is dynamic, in particular RNA-binding is associated with a dilation of the central aperture to accommodate RNA substrate. RNA binding is associated with increased conformational order that may be propagated from the aperture to the active site (Nurmohamed *et al.* 2009). Arg83, close to FFRR loop, may be required for guiding RNA into the active site and perhaps supports a ratchet-like mechanical displacement of the substrate into the active site (Nurmohamed *et al.* 2009).

The overall structure of ΔKH/S1 was similar to that of the full-length PNPase. Superposition of only one monomer of the full-length and ΔKH/S1 PNPase gave an average RMSD of 1.1 Å for 417 C_α atoms. However, the corresponding RMSD were 1.6 Å and 1.7 Å for the others monomers. The top view of the superimposed trimer shows that the ΔKH/S1 PNPase has a larger ring diameter (Fig. 1.3), and that there is a reduction by ~ 7% of buried interface in the absence of KH and S1 domains (Shi *et al.* 2008). This suggests that the structure of ΔKH/S1 is less compact than full-length PNPase. The current model suggests that KH and S1 domains are involved in

RNA-binding domains of *E. coli* PNPase, as shown by a substantial reduction in RNA binding as well as in enzyme activity resulting from the deletion of the mentioned domains (Stickney *et al* 2005.; Briani *et al.* 2007; Matus-Ortega *et al.* 2007). In additon, the crystallographic results also support the hypothesis that the KH/S1 domain in PNPase is involved in trimeric assembly.

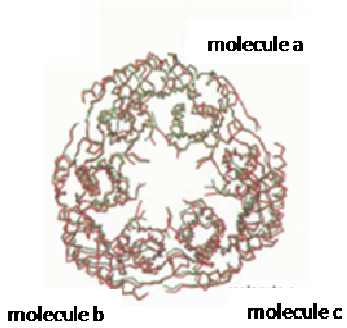

Figure 1.3. Crystal structure comparison between full-length PNPase (green) and truncated mutant ΔKH/S1 (red). One of the monomers (molecule a) in the homotrimer of full-length PNPase was superimposed on ΔKH/S1, giving an average RMSD of 1.1 Å for 417 C_α atoms. The corresponding RMSDs were 1.6 Å and 1.7 Å for the molecules b and c, respectively. ΔKH/S1 is sli ghtly more expanded than full-length PNPase (from Shi *et al.* 2008).

The co-crystal structure of *E. coli* PNPase core and Mn^{2+} , that can substitute for Mg^{2+} to support catalysis (Nurmohamed *et al.* unpublished results), reveals that the metal is coordinated by conserved residues D486, D492 and K494. These residues might play a role not only in acid-base catalysis but also in positioning Mg^{2+} to activate phosphate and to stabilize the transition state (Nurmohamed *et al.* 2009). Furthermore, *E. coli* PNPase has been crystallized in complex with the recognition site from RNase E and with manganese, in the presence or in absence of modified RNA (Nurmohamed *et al.* 2009). The crystallographic data show that only the amino-terminal RNase PH subdomain interacts with RNase E. The observed stoichiometry of one PNPase monomer binding to one RNase micro-domain

in the crystal structures is consistent with data from mass spectrometry (Callaghan *et al.* 2004) and isothermal titration calorimetry, which show that one RNase E micro-domain binds to each PNPase protomer. The interaction may be stronger in the context of the full-length RNase E, since that molecule is a tetramer and therefore the PNPase binding sites might be spatially co-localized. PNPase core and full-length PNPase bind to RNase E with roughly equal affinity (Stickney *et al.*2005). This suggests that the missing KH and S1 domains do not affect the interaction between RNase E and PNPase.

1.2.2 PNPase autogenous regulation

The expression of *pnp* is post-transcriptionally regulated through the control of its messenger stability. The *pnp* primary transcripts are processed by RNase III, which cleaves the RNAs 37 (site 1) and 75 (site 2) nucleotides downstream of the *pnp-p* transcription start point within a long hairpin structure in the 5'-untranslated region (5'-UTR) upstream of the Shine–Dalgarno sequence (Régnier and Grunberg-Manago, 1990; Jarrige, *et al.*, 2001; Robert-Le Meur and Portier, 1992).

PNPase post-transcriptionally regulates its own expression by controlling the stability of the RNase III processed mRNAs: the processed transcript, in the presence of PNPase, becomes very unstable (Portier *et al.*, 1987; Robert-Le Meur and Portier, 1992; Robert-Le Meur and Portier, 1994). Two non-mutually exclusive models have been proposed to mechanistically explain PNPase autogenous regulation. The first postulates that PNPase could bind determinants in the 5'-UTR of *pnp* mRNA and inhibit translation, thus promoting degradation of the transcript (Robert-Le Meur and Portier, 1992; Robert-Le Meur and Portier, 1994). A more recent model

maintains that the duplex formed by the 37 nt long RNA (RNA37) upstream of RNase III cleavage site 1 and the new 5'-monophosphate end of the mature *pnp* mRNA protects the mRNA from degradation (Fig. 1.4a). PNPase would trigger *pnp* mRNA decay by degrading the small RNA37 from the short 3' overhang (Fig. 1.4b) (Jarrige *et al.*, 2001).

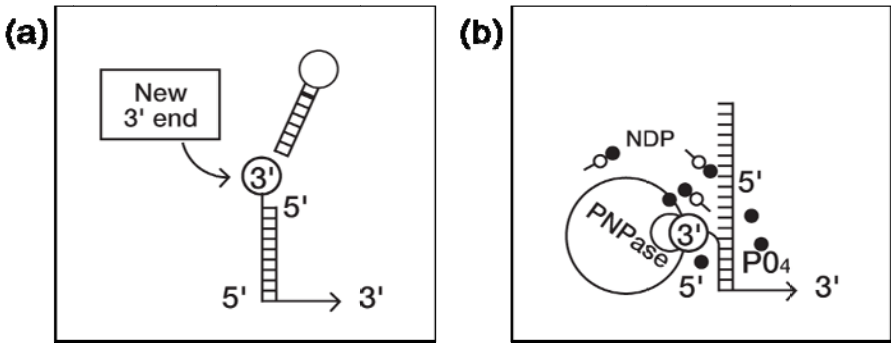

Figure 1.4. (a) Double stranded stable pnp mRNA leader; (b) PNPase removes the upstream branch of the duplex (From Jarrige et al., 2001).

Whether removal of the double stranded structure creates *per se* an unstable transcript or this is just a prerequisite for PNPase-mediated translational repression and subsequent mRNA destabilization, as suggested by the former model, is not clear, as it is not known which RNA decay pathway(s) degrades the "destabilized" *pnp* mRNA.

The bottom half of the stem–loop produced by this cleavage remains double stranded (formed by a small RNA - RNA39 - paired the new 5'-end) both *in vitro* and *in vivo* since it continues to act as a barrier to degradation in the absence of PNPase (Robert-Le Meur and Portier, 1994).

It has been proposed that this mRNA becomes unstable because PNPase binds to the new 5'-end and prevents translation.

More recently, the same and other groups proposed that PNPase and a short duplex remaining at the 5'-end of *pnp* mRNA upon RNase III

processing are the determinants of *pnp* mRNA stability and that both the degradation and RNA binding activity of PNPase are required for autoregulation (Robert-Le Meur and Portier, 1994; Jarrige *et al.*, 2001; Jarrige *et al.*, 2002; Regonesi *et al.*, 2004).

It has been proposed that the dangling 3' end created by RNase III cleavage at the top of the mRNA duplex constitutes a target for PNPase, allowing it to progressively remove the upstream branch of the duplex. This releases a *pnp* mRNA with a single-stranded 5'-end, which is subject to rapid degradation. However, this model presents some problems. First of all, it is known that a single-strand tail longer than six nucleotides is necessary for a fast degradation by PNPase, suggesting that the ssRNA needs a minimum length to reach the catalytic site (Spickler and Mackie, 2000). Then, the two-nucleotide-long protrusion derived from the RNase III digestion on the *pnp* transcript may not be targeted by PNPase unless some other events occur such as spontaneous or RNA-helicase mediated dissociation and/or polyadenylation that generate a single strand filament long enough to interact with PNPase (Spickler and Mackie, 2000).

During cold acclimation such an autogenous control is transiently relieved and *pnp* mRNA becomes extremely abundant mainly because of stabilization (Zangrossi *et al.*, 2000; Beran and Simons, 2001). PNPase level, however, increases two–threefold only after acclimation, when the level of *pnp* mRNA has returned to nearly pre-shock levels (Zangrossi *et al.*, 2000). In addition, polycistronic transcripts extending from *pnp* to the downstream genes *nlpI* and *deaD* are produced, thus indicating that transcription termination at intercistronic intrinsic terminators is transiently suppressed (Zangrossi *et al.*, 2000; Bae *et al.*, 2000).

1.3 The RNA degradosome

The RNA degradosome is a molecular machine involved in RNA regulation that was discovered in two different laboratories during the purification and characterization of *E. coli* RNase E (Carpousis et al., 1994; Py et al., 1994).

Global analyses of RNA steady-state abundance and turnover in *E. coli* indicate that the degradosome has a broad role in gene regulation (Bernstein et al., 2004). Mutants in which degradosome assembly is disrupted have a slow-growth phenotype (Briegel et al., 2005) and altered metabolic profiles. Although disruption of the degradosome affects the levels of many transcripts, some are affected strongly, suggesting that these transcripts might contain a structural or sequence signal for their recognition. Many of these transcripts encode glycolytic enzymes and other proteins involved in processes related to cellular energetics (Bernstein et al., 2004).

1.3.1 Composition of the *E. coli* RNA degradosome

The major components of this multiprotein complex include RNase E, PNPase, RNA helicase B (RhlB), and enolase (For PNPase see above).

RNase E

RNase E (coded by *rne* gene) is an essential enzyme implicated in both maturation of stable RNAs (including rRNA, 9S RNA, tRNA, tmRNA) and degradation of mRNA (Masse *et al.*, 2003). RNase E was initially characterized as an activity required for the processing of 9S rRNA (Ghora and Apirion, 1978). Inactivation of temperature-sensitive *rne* mutants leads not only to accumulation of unprocessed stable RNAs (Ghora and Apirion,

1978; Ow and Kushner, 2002), but also to increased lifetimes for individual mRNAs, as well as for bulk mRNA (Ono and Kuwano, 1979; Cohen and McDowall, 1997; Coburn and Mackie, 1999). In spite of its role in the initiation of mRNA decay, RNase E appears to lack strict sequence specificity and cleaves single-stranded RNA 5' to AU dinucleotides (McDowall *et al.,* 1994).

RNase E, a 1061-amino acid protein, can be divided into three functionally distinct domains: the amino terminal domain (amino acids 1–498), containing the single-strand-specific endonuclease activity; the central domain (residues ~ 500–650), an arginine and proline-rich central region that contains an RNA binding sites; and the carboxy-terminal domain (residues ~ 650-1061), that provides a scaffold for the assembly of RhlB, PNPase and enolase into the RNA degradosome (Ghora and Apirion, 1978; Ow *et al.*, 2000; Ono and Kuwano, 1979; Mudd *et al*. 1990; Babitzke and Kushner, 1991; McDowall and Cohen, 1996) (Fig. 1.5).

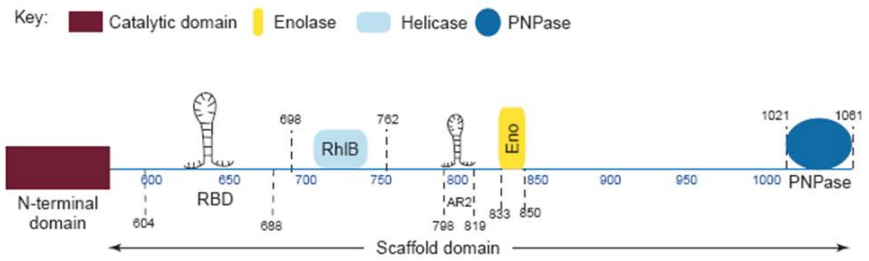

Figure 1.5. Summary of the protein–protein and protein–RNA recognition microdomains of *E. coli* RNase E. Near the recognition sites for helicase (Rhlb) and enolase (Eno) are two arginine-rich regions that might be independently involved in RNA binding: the RNA-binding domain (RBD) and arginine-rich region 2 (AR2). We define 'microdomains' as the short segments on the scaffold domain of RNase E that are required for protein–protein and protein–RNA interaction (From Carpousis, 2007).

The enzyme is a homotetramer and can be viewed as a dimer of dimers. The catalytic domain contains structural subdomains, such as DNase I and RNase H, and an S1 subdomain, which occurs in many different

RNA-binding proteins (Fig. 1.6). The structure of RNase E has allowed a better understanding of many features of the enzyme, including the specificity for single-stranded RNA and the activation of catalytic activity by 5'-monophosphorylated RNA. The overall structure of the tetramer is important for formation of the catalytic site as the monomers by themselves have little or no activity. Other important characteristics include a site forming a pocket that specifically interacts with the terminus of 5'-monophosphorylated RNA and a channel that permits access of single-stranded RNA, but not double-stranded RNA, to the catalytic site (Callaghan *et al.*, 2005). Based on sequence comparisons, residues 37–119 in the N-terminal segment of RNase E are predicted to correspond to an S1 subdomain (Bycroft *et al.*, 1997). In particular, these residues show 30% sequence identity with the S1 domain of PNPase, for which a three-dimensional structure has been determined by NMR spectroscopy. S1 domains are RNA-binding modules, originally identified in the ribosomal protein S1. Beyond an expected role in mediating RNA binding, the precise function of the S1 domain in RNase E is not understood .

Most of the noncatalytic region of RNase E is predicted to be natively unstructured by sequence analysis and by X-ray scattering studies (Callaghan *et al.*, 2004).

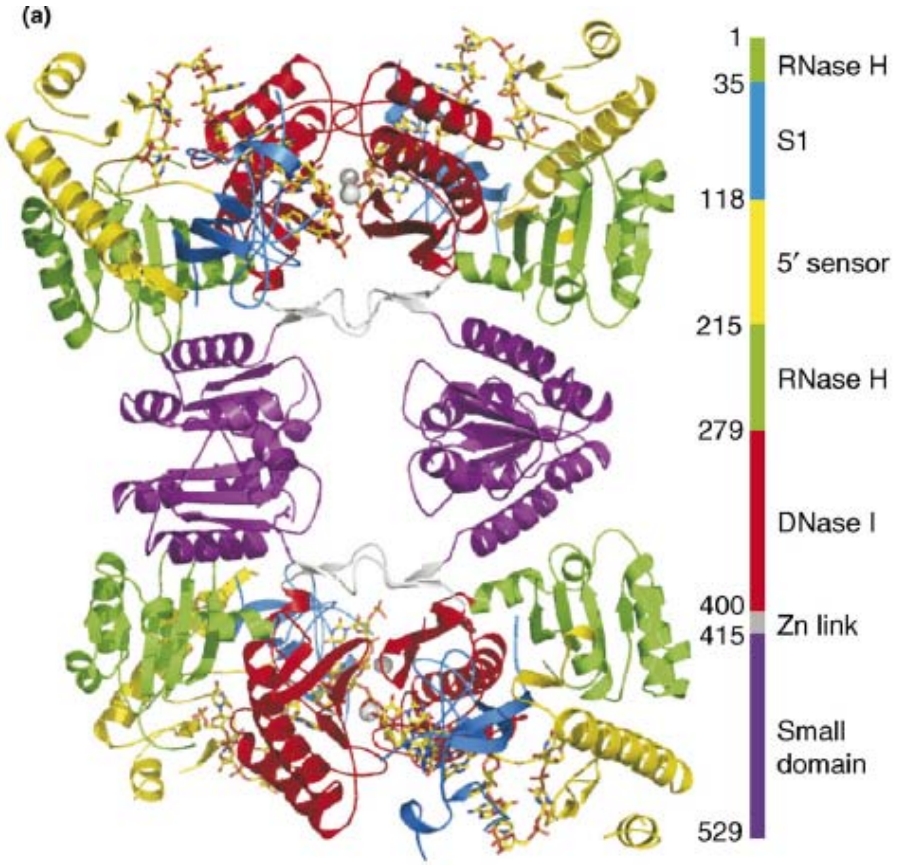

Figure 1.6. Ribbon representation of the homotetramer of the catalytic domain of RNase E from *E. coli*. The different subdomains of the four protomers revealed by the structure are shown as indicated in the colour key. (From Worrall and Luisi, 2007)

Enolase

The 48 kDa enolase is a universally conserved enzyme of glycolytic metabolism that is found in organisms of all three domains of life, namely, the Archaea, Bacteria and eukaryotes. The enzyme catalyses the interconversion of phosphoenolpyruvate and 2-phospho-D-glycerate, which proceeds through the reversible elimination of water. In *E. coli*, roughly

one-tenth of the total enolase is in the RNA degradosome (Py *et al.*, 1996). While the role of the other degradosome components is understood, the role of enolase is not clear. However, an analysis of transcript levels using DNA microarrays has shown that disruption of enolase interaction with RNase E in *E. coli* has consequences on the bulk turnover of mRNA, and in particular, on transcripts encoding enzymes of the energy-generating metabolic routes (Lee *et al.*, 2002). It has also been observed that the association of enolase with RNase E is required for the response to excess phosphosugar (Morita *et al.*, 2004; Kawamoto *et al.*, 2005). This response involves the induction of a small regulatory RNA, *sgrS* which is recruited to the degradosome *via* the small RNA binding protein, Hfq, resulting in the targeted destruction of the transcript encoding the transmembrane glucose transporter, *ptsG* (Morita *et al.*, 2005). The physical interaction of enolase and RNase E is not required for the induction of small regulatory RNA or the transcript turnover, so it remains unclear how enolase functions in the degradosome. One possible function of enolase is the localised generation of phosphoenolpyruvate for an activating phosphotransfer reaction. Although it remains to be established, the function of enolase in the degradosome may serve to link the cellular metabolic status with post-transcriptional gene regulation. Recently Luisi and co-workers (Chandran *et al.*, 2006) has co-crystallized enolase with a synthetic peptide corresponding to residues 833 to 850 from RNase E, which earlier studies have shown to lie within a recognition region mapped by yeast two-hybrid assay (Vanzo *et al.*, 1998) and to be sufficient for binding enolase in solution (Callaghan *et al.*, 2004). Enolase is a stable dimer in solution and in the crystal, and in the co-crystals of the enolase/peptide complex, two such dimers occupy the asymmetric unit. In both dimers, a well-ordered RNase E peptide penetrates an inter-protomer groove (Fig. 1.7). The complex was

also crystallized in three other crystal forms with different symmetry and in all three of these cases, the density for the peptide is averaged over two non-equivalent positions in the central cleft (Chandran *et al.*, 2006). While this made it difficult to develop a model, it was nonetheless clear that the peptide occupies the same site in all crystal forms, even under different crystallisation conditions. The peptide intersects the molecular dyad of the enolase dimer to make non-equivalent contacts with the two protomers and leaving insufficient space for a second peptide. The observed stoichiometry of one RNase E peptide bound by one enolase dimer is consistent with the observations from non dissociating mass spectrometry (Callaghan *et al.*, 2004). As RNase E is a homotetramer (Callaghan *et al.*, 2003; Callaghan *et al.*, 2005), it can in principle bind up to four enolase dimers. However, enolase binding may exclude other degradosome components from the same RNase E protomer (Morita *et al.*, 2005), so the exact stoichiometry of enolase in the context of the degradosome awaits experimental elucidation. The enolase structure can be divided into two architectural components (Fig.1.7), which are labelled as the N-terminal domain and barrel domain. The deep cleft where the RNase E peptide binds is formed between the N-terminal domains of the individual enolase protomers. The geometry of this cleft and the dimerization surface are well conserved when comparing enolase from eukaryotes and prokaryotes.

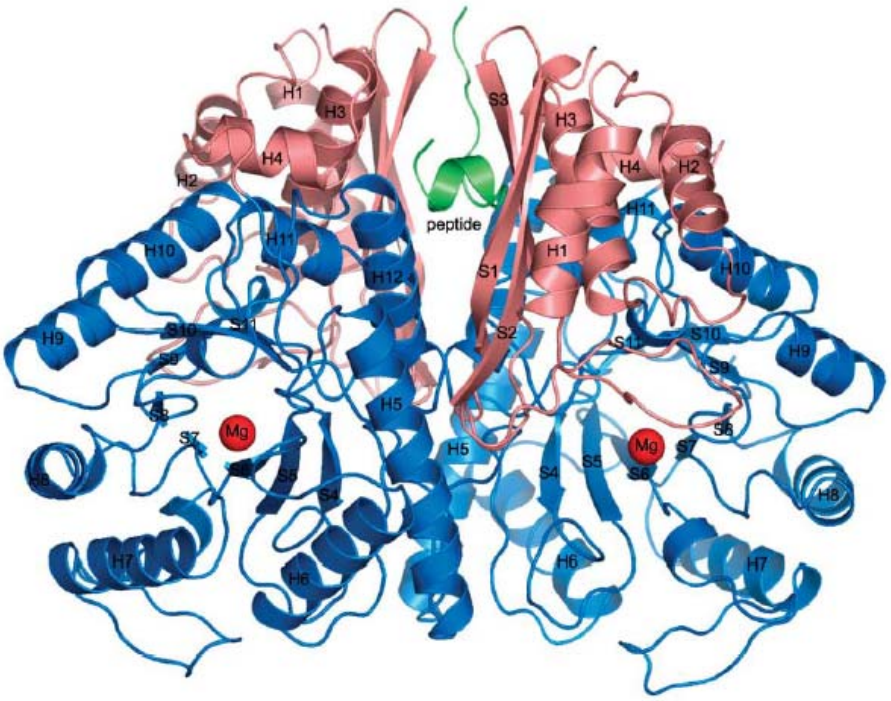

Figure 1.7 The interaction of enolase and RNase E. A schematic representation of the crystal structure of the enolase dimer in complex with its recognition segment from RNase E. The red sphere is a hydrated magnesium ion that occupies the active site (From Kuhnel *et al.*, 2001).

RhlB

RhlB is a DEAD-box RNA helicase (Kalman *et al.*, 1991) that facilitates the degradation of structured mRNA decay intermediates by PNPase in the RNA degradosome (Py *et al.*, 1996; Coburn *et al.*, 1999; Khemici *et al.*, 2004). This activity, which requires ATP hydrolysis, is believed to involve the local unwinding of secondary RNA structures that block PNPase (Carpousis *et al.*, 1999). Multienzyme ribonucleolytic complexes in other organisms have also been shown to interact with DEAD-box or related proteins (Symmons *et al.*, 2002). The DEAD-box proteins are a family of putative RNA helicases that generally have RNA-dependent ATPase activity *in vitro*. They contain a characteristic set of conserved sequence motifs that were

discovered in a comparison between the eukaryotic translation initiation factor eIF4A and the *E. coli* protein SrmB (Nishi *et al.*, 1988). eIF4A is involved in loading the eukaryotic small ribosomal subunit onto mRNA (Rogers *et al.*, 2002). SrmB is a chaperone in the assembly of the large ribosomal subunit of *E. coli* (Charollais *et al.*, 2003). The DEAD-box proteins are now known to be part of the ubiquitous DEAD box family of helicases that participate in many RNA unwinding and remodelling reactions (Tanner *et al.*, 2001). The DEAD box proteins, together with other RNA and DNA unwinding enzymes, constitute a superfamily containing a structurally conserved ATPase domain with RecA-like architecture (Caruthers *et al.*, 2002). This domain is likely to be a generic motor for the unwinding and remodelling of nucleic acids. RhlB and eIF4a, which are among the smallest members of the DEAD box family, contain little more than this conserved catalytic core. The DEAD box domain often associates with additional domains, either covalently in the same polypeptide or non-covalently within a multienzyme complex. RhlB and eIF4A are DEAD box helicases that require a protein partner for biological activity (Silverman *et al.*, 2003). Recently, Khemici *et al.* (2005) have studied *in vivo* the role of RhlB in the degradation of a *lacZ* mRNA transcribed by bacteriophage T7 RNA polymerase (T7-*lacZ* mRNA). Because the phage polymerase is 8-fold faster than its *E. coli* counterpart, transcription outpaces translation, producing long stretches of ribosome-free RNA. This message is exceptionally sensitive to inactivation and degradation by RNase E (Iost and Dreyfus, 1995). The integrity of the non catalytic region of RNase E, including the sites that bind RhlB and enolase, is necessary for this sensitivity (Lopez *et al.*, 1999; Leroy *et al.*, 2002). Deleting the RhlB gene stabilizes the T7-*lacZ* mRNA, leading to a significant increase in β-galactosidase synthesis. This is evidence that RhlB

is part of a specialized pathway involved in the degradation of ribosome-free mRNA by RNase E (Khemici *et al.*, 2005).

1.3.2 Subassembly of the RNA degradosome

Recently, Marcaida *et al.* (2006) proposed a model of the degradosome that integrates the crystallographic and biochemical data (Fig. 1.8). They suggested that intrinsically unstructured tails emanate from the tetrameric catalytic domain of RNase E, which can accommodate up to four enolase dimers and four helicase monomers. Because a PNPase trimer can bind three RNase E scaffolding tails, accommodating all interaction sites would require a ratio of three RNase E tetramers to four PNPase trimers. We can envisage that the scaffolding tails of RNase E cooperate to build the degradosome assembly and perhaps to form proximal surfaces for shared binding of RNA substrates. Including enolase and helicase, the degradosome would have a molecular mass in excess of 4.1 MDa (which is greater than a ribosome) and would readily qualify as a supramolecular machine dedicated to RNA processing and turnover. It is not clear whether all of the components can be accommodated simultaneously (Morita *et al.*, 2005).

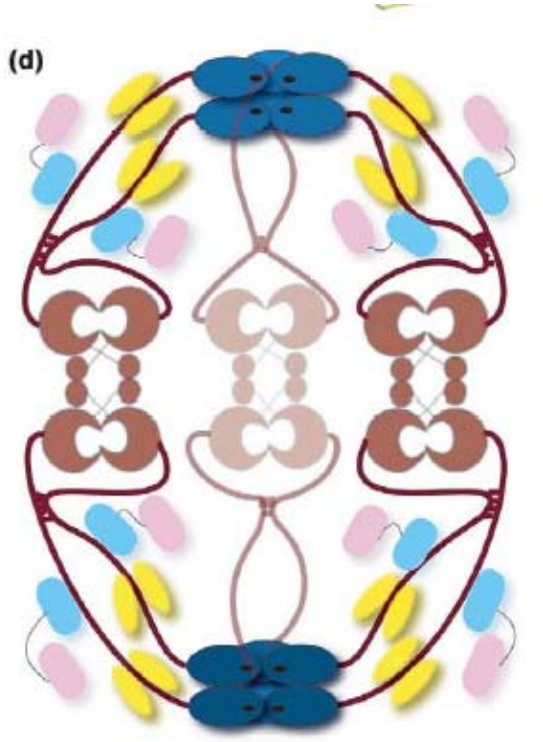

Figure 1.8 Model of degradosome assembly based on crystallographic and biophysical data. To satisfy all of the available binding sites, a ratio of four PNPase trimers (blue) to three RNase E tetramers (brown and tan) is required. The enolase dimers are yellow and the helicase domains are pink (N-terminal domain) and cyan (C-terminal domain). The symmetry of the tetrameric RNase E and trimeric PNPase can be matched if two PNPase trimers stack together to generate a local twofold axis, such that pairs of RNase E tails (brown and tan) make equivalent contacts with each trimeric ring. A set of PNPase trimers stack precisely in this manner in the crystal lattice of the *S. antibioticus* enzyme (Symmons et al., 2002), and these rings associate in such a way that the RNA-binding surfaces are exposed and could engage RNA substrates. The pairwise interactions of the C-terminal tails, implicated from yeast two-hybrid experiments (Vanzo *et al*., 1998) are indicated by short connecting lines. The degradosome complex might in fact have 'quasi-equivalent' symmetry if the scaffolding tails do not bind all of the components simultaneously. (From Marcaida *et al*., 2006)

1.4 Aim of the work

The present work was originally undertaken to further clarify the mode of assembly and the regulation mechanisms of the RNA degradosome, a protein machinery that controls RNA turnover. However, during these studies we observed an inhibitory effect by ATP on PNPase. So we focused

on this phenomenon, attempting to clarify its mechanism and physiological role(s). Searching for nucleotide-binding sites, in the latest stage of the work we also investigated the mode of interaction between the enzyme and both nucleotide and RNA substrates.

2. MATERIALS AND METHODS

2.1 Strains and grown conditions

C-5691 (C-1a D*pnp-751*), which carries an in frame deletion encompassing about 95% of *pnp* coding sequence (coordinates 7740-5709, GenBank Accession Number AE000397), was obtained by allele replacement as described by Datsenko and Wanner (2000). In brief, an FRT-flanked kanamycin resistance cassette was amplified by PCR from plasmid pKD13 with primers FG738 (*ATCGTTCGTAAATTCCAGTACGGCCAACACACC GTGACT*ATTCCGGGGATCCGTCGACC; AE000397: 7779-7741 followed by pKD13 priming site 4) and FG739 (*AGCAGCCGGAGCTTCCGGTGCTGCAGCAG GTTGAGACT*GTGTAGGCTGGAGCTGCTTC; AE000397: 5671-5708 followed by pKD13 priming site 1). BW25113 competent cells, carrying pKD46 helper plasmid, which expresses k Red (*gam*, *bet*, *exo*) function, were transformed by electroporation with 200 ng of gel-purified PCR fragment and plated at 37 °C. Colonies were tested for both the presence of the D*pnp*::*kan* allele at the *pnp* locus in the chromosome and the loss of the helper plasmid. The D*pnp-751*::*kan* mutation was then transferred in *E. coli* C-1a by P1 transduction (Regonesi *et al.*, 2004), obtaining strain C-5690. To excise the KanR cassette from the *pnp* mutant, C-5690 was transformed with the temperature-sensitive plasmid pCP20, which encodes the FLP recombinase, thus promoting recombination between the FRT sites (Briani *et al*., 2002).A few transformants were purified at 42°C and tested for the loss of both the KanR cassette and plasmid 152 (*Regonesi et al. 2006) 151–161* pCP20. The presence of the D*pnp-751* mutation (strain C-5691) was confirmed by Southern blotting and sequencing of the PCR-amplified *pnp* region. D*pnp-751* encodes a 60 aa long fusion peptide formed by the first 16 and the last

17 residues of PNPase flanking a 27 aa-long internal sequence coded by the "scar" DNA left by the FLP-promoted recombination event. C-5691(DE3) was obtained by lysogenization of C-5691 with phage DE3, a k derivative carrying the T7 RNA polymerase gene under p*lac*UV5 promoter (Studier and Moffatt, 1986). The strain was transformed with plasmids pRE196 (FLAG-Rne; kindly provided by S. Lin-Chao) and pAZ8 (*pnp+*) or pAZ12 (*pnp-701*), previously described (Symmons, *et al*., 2000; Jarrige *et al*, 2002; Beran and Simons, 2001).

The *Escherichia coli C* strains used are shown in Table 2.1 and the plasmids in Table 2.2.

Table 2.1. *E. coli* strains

Strains	**Important notes**	**References**
C-5691	*pnp*-751	Regonesi *et al.*, 2006
C-5691(DE3	Phage DE3 is k derivative carryng the T7 Rna polymerasse gene	Briani *et al.*, 2007
C-5691 (DE3)/pRE196	Plasmid pRE196 carryng the Rnase E-FLAG gene (Mizak, 1996)	Regonesi *et al.*, 2006

Table 2.2. Plasmids used

Plasmids	mutations	References
pAZ8	wt	Regonesi *et al.*, 2006
pAZ121	E81D	Briani *et al.*, 2007
PAZ122	E81K	Briani *et al.*, 2007
pGC400	Wt	Del Favero *et al.*, 2008
pET22b-102/103	R79/80A	Shi *et al.,* 2008
pET22b-106	R83A	Shi *et al.,* 2008
pGC1101	F77A	
pGC1102	F78A	
pGC1103	R79A	
pGC1104	F56A	
pGC1105	R93A	
pGC1106	F103A	
pGC1107	R80A	
pGC1108	R83A	
pGC1109	R79AR80A	

2.1.1 Culture media

The media of choice for the growth of cells is LD medium and LD agar, each containing 50 μg/ml ampicillin and 25μg/ml chloramphenicol.

LD medium:

Peptone: 10 g/l

Yeast extract: 5 g/l

NaCl: 10 g/l

Ampicillin: 100 mg/l

LD agar :

Peptone:	10 g/l
Yeast extract:	5 g/l
NaCl:	10 g/l
Ampicillin:	100 mg/l
Agar:	10 g/l

Ampicillin stock solution: 50 mg/ml in sterile water, store in aliquots at -20°C. Chloramphenicol stock solution: 25 mg/ml in ethanol, store at -20°C

2.1.2 Transformation of *E. coli* C5691(DE3)

The following procedure is frequently used to prepare batches of competent bacteria that yield 5 x 10^6 to 2 x 10^7 transformed colonies per microgram of supercoiled plasmid DNA.

Pick a single colony from a plate and transfer it into 100 ml of LB medium. Incubate the culture for 3 h at 37°C with vigorous shaking. For efficient transformation, it is essential that the number of viable cells should not exceed 10^8 cells/ml. To monitor the growth of the culture, determine the OD_{600} every 20-30 min.

Aseptically transfer the cells to sterile, disposable, ice-cold 50-ml polypropylene tubes (Falcon 2070). Cool the cultures to 0°C by storing the tubes on ice for 10 min. Recover the cells by centrifugation at 4000 rpm for 15 min at 4°C in a Haraeus Sephatec 2252 rotor. Decant the media from the cell pellets and resuspend each pellet in 2.5 ml of ice-cold MOPS I solution and store on ice. Recover the cells by centrifugation at 4000 rpm for 10 min at 4°C. Decant the fluid from cell pellets and resuspend each pellet in 2.5 ml of ice-cold MOPS II solution and store on ice for 15 min. Recover the cells by

centrifugation at 2000 rpm for 20 min at 4°C. Resuspend each pellet in 500 µl of MOPS II solution.

Using a chilled, sterile pipette tip, transfer 200 µl of each suspension of competent cells to a sterile microfuge tube. Add DNA (10 ng) to each tube. Mix contents of tubes by swirling gently. Store the tubes on ice for 30 min. Transfer the tubes to a rack placed in a circulating water bath that has been preheated to 42°C. Leave the tubes in the rack for exactly 30 s. Rapidly transfer the tubes on ice and allow the cells to chill for 1-2 min. Add 5 ml of LB medium to each tube. Incubate the cultures for 1 h at 37°C. Recover the cells by centrifugation at 4000 rpm for 15 min at 4°C and resuspend with 200 µl of LB medium. Transfer the appropriate volume of transformed competent cells onto LB agar plates and incubate at 37°C for 12-16 h.

Solution

MOPS I: 10 mM MOPS, pH 7.0, 10 mM RbCl

MOPS II: 0.1 M MOPS, pH 6.5, 50 mM $CaCl_2$, 10 mM RbCl

2.2 Growth, collection and storage

E. coli cultures were grown in a rotatory shaker at 37 °C in LD broth (Ghisotti *et al*., 1992) supplemented with ampicillin (100 µg/ml) and chloramphenicol (30 µg/ml) if required, up to mid exponential phase (OD_{600} = 0.8). Under these conditions FLAG-Rne was expressed at its basal level from pRE196.

The strains transformed with plasmids pGC400 and derivates were induced with 0.4 mM IPTG (OD_{600}= 0.4-0.5) for three hours.

Cells were harvested by centrifugation for 10 min at 6000 rpm and 4°C, washed with 50 mM Tris–HCl, pH 7.4 and stored at –20 °C.

Centrifuge: Beckman Coulter Avanti J-20 centrifuge, rotor JA20 e rotor JA10.

2.3 Purification of PNPase wild type and mutant

2.3.1 Cell lysis

Following harvest, cell pellets were resuspended in 20mL Buffer A and centrifuged again as described above. The cell pellets were then frozen for at least 45 min at 20°C. The pellets were thawed by uspension in 20 mL cold Buffer A and 28 mg each of lysozyme and CHAPS were added. The suspensions were mixed gently by inversion, 675 U DNase I (in 100 l L Buffer A) was added, and the suspensions were incubated on ice for 60 min. The incubated suspensions were then centrifuged for 15 min at 15,000g and 4 _C. The supernatants were removed and in some cases stored overnight at -20°C.

Buffer A:

50mM Tris–HCl, pH 8.0, 5mM $MgCl_2$, 1mM dithiothreitol, 5% glycerol, and one tablet in 100 mL of the Roche Complete protease inhibitor cocktail.

2.3.2 Ion-exchange chromatography

For the purification was used an ion-exchange chromatography (DEAE-Sephacel, Invitrogen)

Procedure

• Pack 2ml of DEAE-Sephacel into the column and equilibrate with Tris/HCl 25 mM pH 8.0 (10 volumes).

- Apply the supernatant onto the column (2ml/h)
- Wash with 5 volumes of buffer A
- Elute with 5 volumes of NaCl linear gradient (0-0.5 M)

2.4 Purification of FLAG-Rne degradosome

FLAG-Rne degradosomes were prepared as described (Grunberg-Manago *et al*., 1999) with minor modifications. Frozen cell paste (from 0.5 to 5 g) was broken in lysozyme–EDTA buffer [1 ml/g cell; 50 mM Tris–HCl, pH 7.4, 100 mM NaCl, 5% glycerol, 3mM EDTA, 1mM dithiothreitol (DTT), 1.5 mg/ml lysozyme (Sigma, St. Louis, MO, USA), 1 mM PMSF, Complete ™ EDTA-free protease inhibitor (1 tablet/50 ml; Roche, Mannheim, Germany)] by vortexing three to four times for 1 min after increasing intervals (10–20–40 min) of incubation in ice. DNase-Triton buffer [50 mM Tris–HCl, pH 7.4, 100mM NaCl, 5% glycerol, 1 mM DTT, 30 mM magnesium acetate, 3% Triton X 100, 1 mM PMSF, 20 µg/ml di DNase I (Sigma), Complete™ EDTA-free protease inhibitor was then added (0.5 ml/g cell), the suspension was incubated 30 min at room temperature, and 5M NH_4Cl was slowly added with stirring at 4 °C (final concentration 1.25 M). The lysate was then incubated for additional 30 min and clarified by centrifugation at 20,000 × *g* for 60 min. The supernatant was precipitated with ammonium sulfate (40% saturation) and the pellet resuspended in binding buffer (50 mM Tris–HCl, pH 7.4, 150 mM NaCl; 5% glycerol, 1 mM EDTA, 1 mM PMSF, 0.1% Genapol X-80, Complete™ EDTA-free protease inhibitor; 1 ml/g cell). The resuspended pellet was applied to an Anti-FLAG® M2 Affinity gel column (Sigma), bed volume 0.5 ml, pre-activated with 3 volumes of 0.1 M glycine HCl, pH 3.5, and equilibrated with 10 volumes of binding buffer. The column was washed with 5 volumes of binding buffer and the degradosome was eluted with 3 volumes of binding buffer containing 150 µg/ml FLAG-

PEPTIDE (Sigma); 0.5-ml fractions were collected and stored in 50% glycerol at –20 °C.

2.5 Protein content determination

Protein content was determined using the Bradford method (Rockford, IL). The Bradford assay works by the action of Coomassie brilliant blue G-250 dye (CBBG). This dye specifically binds to protein at arginine, tryptophan, tyrosine, histidine and phenylalanine residues. CBBG binds to these residues in the anionic form, which has an absorbance maximum at wave length of 595 nm. The assay is monitored at 595 nm in a spectrophotometer, and measures the CBBG complex with the protein. Thus Beer's Law may be applied for accurate quantification of protein by selecting an appropriate dye volume to sample concentration ratio. Bovine plasma immunoglobulin was used as standard protein.

2.6 SDS polyacrylamide gel electrophoresis

Proteins are amphoteric compounds; their net charge therefore is determinated by the pH of the medium in which they are suspended. In a solution with a pH above its isoelectric point, a protein has a net negative charge and migrates towards the anode under an electric field. Sodium dodecyl sulphate (SDS) is an anionic detergent which denatures proteins by "wrapping around" the polypeptide backbone. Doing so, SDS confers a negative charge to the polypeptide in proportion to its length. It is usually necessary to reduce disulphide bridges in proteins before they adopt the random-coil configuration necessary for size separation. In denaturing SDS-PAGE separation therefore, migration is not by intrinsic electrical charge of the polypeptide, but by molecular weight. We utilized the discontinuous

system in which a non-restrictive large pore gel, called a stacking gel, is layered on top of a separating gel called a running gel.

- Running gel al 10% (10 ml)

Acrylamide 40%/metilen BIS 37.5:1 (Ambion,USA)	2.5 ml
1.5 M Tris/HCl, pH 8.8, 0.4% SDS	2.5 ml
Water	4.92 ml
Ammonium persulfate (100 mg/ml)	73 µl
TEMED	5 µl

- Stacking gel al 4% (5 ml)

Acrylamide 40%/metilen BIS 37.5:1 (Ambion,USA)	0.5 ml
0.5 M Tris/HCl, pH 6.8, 0.4% SDS	1.32 ml
Water	3.15 ml
Ammonium persulfate (100 mg/ml)	25 µl
TEMED	8.35 µl

Electrophoresis buffer

The final buffer composition is 196 mM glycine; 0.1% SDS; 50 mM Tris-HCl, pH 8.3, made by diluting a 10 X stock solution.

- Sample Buffer 5X

0.5 M Tris/HCl, pH 6.8	2.5 ml
10% SDS	1.0 ml
Glycerol	1.0 ml
2-mercaptoethanol	0.25 ml
Water	0.25 ml

Separation under native condition

In native electrophoresis protein migration depends on the intrinsic electrical charge of the polypeptide and the molecular weight.

The polyacrylamide concentrations of running and stacking gels are 10% and 4%, respectively.

Gel staining

We utilized the Gel-Code® method that is based on Coomassie Blue property. Coomassie™ Blue staining is based on the binding of the dye Coomassie Brilliant Blue R-250 which binds non-specifically to virtually all proteins. Coomassie Blue binds to proteins approximately stoichiometrically, so this staining method is preferable when relative amounts of protein need to be determinate by densitometry. The gel is first washed in water and then incubated for 1 h in Gel-Code Blue Stain Reagent (Pierce, Rockford, IL), finally it is washed from the background.

2.7 Cyclic assay of PNPase

The assay devised by Fontanella (1998) was performed on a mixture containing, in a volume of 1.5 ml, 50mMTris–HCl, pH 7.4, 0.1MKCl, 5mMMgCl2, 20 mg/ml polyA, 1.5 mM phosphoenolpyruvate, 20 mM glucose, 0.5mMNAD1, 0.6 U/ml pyruvate kinase, 2 U/ml hexokinase, 4 U/ml glucose-6-phosphate dehydrogenase, and suitable amounts of cell extracts (typically, 20 to 80 mg protein) and/or pure enzyme. Stock solutions of pyruvate kinase were prepared by a twofold dilution in the assay buffer of the commercially available ammonium sulfate suspension. A clear solution was thus obtained, in which pyruvate kinase was stable over several months. This made it possible to add exact amounts of enzyme to each

assay mixture, an essential prerequisite for the reproducibility of the test (see “Theoretical background”). The assay mixtures were prepared immediately before use. Absorbance was continuously recorded at 340 nm and 25°C. After recording the baseline for about 10 min, the reaction was started by addition of 0.75Mphosphate, pH 7.4, to attain a 10 mM final concentration. The slight linear increase that took place before phosphate addition was extrapolated and subtracted from the exponential increase detected thereafter. Alternatively, absorbance of the blank (without phosphate added) was directly subtracted using a dual beam spectrophotometer. Absorbance was then plotted at intervals of 2 min as a function of the square of the reaction time. In such plots, after a short lag time, profiles were linear for at least 15 min, whereas later a decline in linearity was observed. The slope was determined using a suitable linear regression method of an Enzfitter Elsevier-Biosoft program. Pure PNPase was also assayed as described by Godefroy with minor modifications. In a volume of 1.5 ml, the assay mixture contained 50 mM Tris–HCl, pH 7.4, 0.1 M KCl, 5 mM MgCl2, 20 mg/ml polyA, 1 mM phosphoenolpyruvate, 0.1 mM NADH, 1.3 U/ml pyruvate kinase, 10 U/ml lactate dehydrogenase, and suitable amounts of pure enzyme. The reaction was started by addition of phosphate to a 10 mM final concentration. Absorbance was continuously recorded at 340 nm and 25°C. In both assays, polyA and phosphate concentrations were largely saturating and each activity value was obtained from the mean of at least three independent determinations. Standard deviations never exceeded 10% of the respective mean values. One unit of enzyme activity is defined as the amount of enzyme which releases 1 mmol of ADP/min under the working conditions.

Theoretical Background

The assay relies on the following reaction scheme:

$$\text{Poly(A)}_n + \text{Pi} \xleftrightarrow{\text{PNPase}} \text{poly(A)}_{n-1} + \text{ADP}$$

$$\text{ADP} + \text{PEP} \xleftrightarrow{\text{PK}} \text{ATP} + \text{piruvate}$$

$$\text{Glucose} + \text{ATP} \xleftrightarrow{\text{Hexochinase}} \text{Glucose 6-phosphate} + \text{ADP}$$

$$\text{Glucose 6-phosphate} + \text{NAD}^+ \xleftrightarrow{\text{G6PD}} \text{6-Phosphogluconate} + \text{NADH}$$

The rate of appearance of ADP is given by the following equation:

(1) $d[ADP]/dt = A_{PN} - A_{PK} + A_{HK}$

where t is the reaction time, A_{PN} is PNPase activity, A_{PK} is the rate of ADP subtraction by pyruvate kinase, and A_{HK} is the rate of ADP regeneration by hexokinase. Since pyruvate kinase activity is limiting with respect to that of hexokinase, A_{HK} equals A_{PK}, so the Eq. (1) may be rewritten as follows:

(2) $d[ADP]/dt = A_{PN}$

whose integrated form is:

(3) $[ADP] = A_{PN}t + [ADP]_0$

where $[ADP]_0$ is the starting ADP concentration, when t= 0. However, $[ADP]_0$= 0 under our working conditions, as we subjected cell extracts to

extensive dialysis prior to assay. Thus, the Eq. (3) may be simplified as follows:

(4) $[ADP] = A_{PN}t$

Furthermore, the overall reaction rate, detected by measuring the appearance of NADH, equals the rate of the step catalyzed by pyruvate kinase, due to the fact that the activity of this enzyme is limiting with respect to both hexokinase and glucose-6-phosphate dehydrogenase.

If one also assumes that the Michaelis constant of pyruvate kinase for ADP (0.3 mM) is much higher than the concentration of the nucleotide under the assay conditions, then the reaction rate will be given by:

(5) $d[NADH]/dt=(V_{PK}/K_{PK})\,[ADP]$

where V_{PK} and K_{PK} are the apparent maximal velocity and Michaelis constant, respectively. If the Eq. (4) is replaced into the Eq. (5), it follows that:

(6) $d[NADH]/dt=(V_{PK}/K_{PK})\,A_{PN}\,t$

Integrating this equation gives:

(7) $[NADH]=(V_{PK}\,A_{PN}\,t^2)/2K_{PK} + [NADH]_0$

Since at zero time NADH is absent, the Eq. (7) may be rewritten as follows:

(8) $[NADH]=(V_{PK} A_{PN} t^2)/2K_{PK}$

This relationship states that, when plotting [NADH] versus t^2, a linear increase of [NADH] should be observed, with a slope proportional to both PNPase and pyruvate kinase activities. All these predictions were confirmed by our results, which support the theoretical model. In addition, endogenous ATPase should not cause any appreciable interference because its activity was substantially lower than that of hexokinase added to the assay mixture.

Uvikon Spectrophotometer 930 (Kontron Instruments).

2.8 PNPase kinetic assays

2.8.1 Phosphorolytic activity

The phosphorolytic activity using polyA as a substrate was measured in a coupled pyruvate kinase/lactate dehydrogenase assay (Fontanella *et. al*. 1999).

The assay, which measured the ADP produced as NADH oxidation, was performed at 28°C in a 1-ml reaction mixture containing: 50 mM Tris–HCl, pH 7.4, 0.1 M KCl, 30 mg/ml polyA, 1 mM phosphoenolpyruvate, 20 mM glucose, 0.2mM NADH, 1.3 U/ml pyruvate kinase, 10 U/ml lactic dehydrogenase, 2µg/ml PNPase, at the various concentrations of $MgCl_2$, P_i and ATP; and adsorbance was continuosly recorded at 340 nm. One unit of enzyme activity is defined as the amount of enzyme that releases 1 µmol of ADP/min under the working conditions.

$$\text{poly(A)}_n + \text{Pi} \overset{\text{PNPase}}{\leftrightarrows} \text{poly(A)}_{n-1} + \text{ADP}$$

$$\text{ADP} + \text{PEP} \overset{\text{PK}}{\rightarrow} \text{ATP} + \text{pyruvate}$$

$$\text{pyruvate} + \text{NADH} \overset{\text{LDH}}{\rightarrow} \text{lactate} + \text{NAD}$$

2.8.2 Polymerization activity

PNPase polymerization activity was detected by measuring the P_i released during the polymerization reaction (Webb, M. R. 1992) using the ENZCheck phosphate assay kit (Invitrogen). Assay was performed at 25°C in a 1-ml volume containing 50 mM Tris/HCl (pH 7.5), 20 µg/ml polyA, 1 mM MESG, 1 U/ml Purine nucleoside phosphorilase, 2µg/ml PNPase, at the various concentrations of $MgCl_2$, ADP and ATP. Adsorbance was continuosly recorded at 360 nm.

$$\text{poly(A)}_n + \text{ADP} \overset{\text{PNPase}}{\rightleftharpoons} \text{poly(A)}_{n-1} + P_i$$

$$P_i + \text{MESG} \overset{\text{PurNPase}}{\longrightarrow} \text{ribose 1P} + \text{2-amino-6-mercapto-7-methylpurine}$$

2.9 Mutant production

2.9.1 Site-directed mutagenesis

Site-directed mutagenesis experiments is used to insert point mutations and delete or insert single or multiple amino acids. Site-directed mutagenesis is performed using *PfuTurbo*™ high fidelity DNA polymerase. The QuickChange site-directed mutagenesis kit (Stratagene, La Jolla, CA) was used to insert or delete some restriction sites in order to produce different PNP variants, using a normal site-directed mutagenesis protocol (Stratagene, La Jolla, CA) (Fig. 2. 4). PCR products were, then, digested with the

restriction enzyme *Dpn I* (Roche, Milan, Italy) to remove parental DNA. DNA was then used to transform *E. coli* strains.

PRIMER DESIGN:

The mutagenic oligonucleotide primers for use in this protocol must be designed individually according to the desired mutation. The following considerations should be made for designing mutagenic primers:

Both of the mutagenic primers must contain the desired mutation and anneal to the same sequence on opposite strands of the plasmid.

Primers should be between 25 and 45 bases in length, with a melting temperature (*T*m) of ≥78°C.

The desired mutation (deletion or insertion) should be in the middle of the primer with ~10–15 bases of correct sequence on both sides.

The primers optimally should have a minimum GC content of 40% and should terminate in one or more G or C bases.

The following formula is commonly used for estimating the T_m of primers:

T_m= 81.5+ 0.41(%GC) - 675/N - % mismatch

Where *N* is the primer length in bases and values for %GC and % mismatch are whole numbers.

PCR REACTION:

DNA template (10 ng/μl)	2 μl
dNTP mix (10mM)	1 μl
Primers (25 ng/μl)	5 μl
Pfu Ultra buffer 10X	5 μl
Molecular grade water	36 μl
PfuUltra DNA polimerase (2.5 U/μl)	1 μl

Table 2.3. Reaction conditions

Segment	Temperature	Time	Number of cycles
1	95°C	30 sec.	1,00
2	95°C	30 sec.	12 - 18
	55°C	1 min.	
	68°C	1min/Kb plasmid lenght	

Adjust segment 2 of the cycling parameters in accordance with the type of mutation desired (see table 2.4):

Table 2.4. Cycling parameters

Type of mutation desired	Number of cycles
Point mutation	12
Single amino acid change	16
Multiple amino acid deletions or insertions	18

PCR PRODUCTS DIGESTION

Add 1 μl of *Dpn I* (10 U/μl) to reaction mix and incubate at 37°C for 1 h in order to digest parental DNA.

PCR: Mastercycler gradient, eppAG 22331 (Hamburg).

Centrifuge: Eppendorf 5804 R, (Hamburg); Eppendorf 5415 (Hamburg).

Immersion thermostat: HAAKE F3 (Gebrüder HAAKE GmbH).

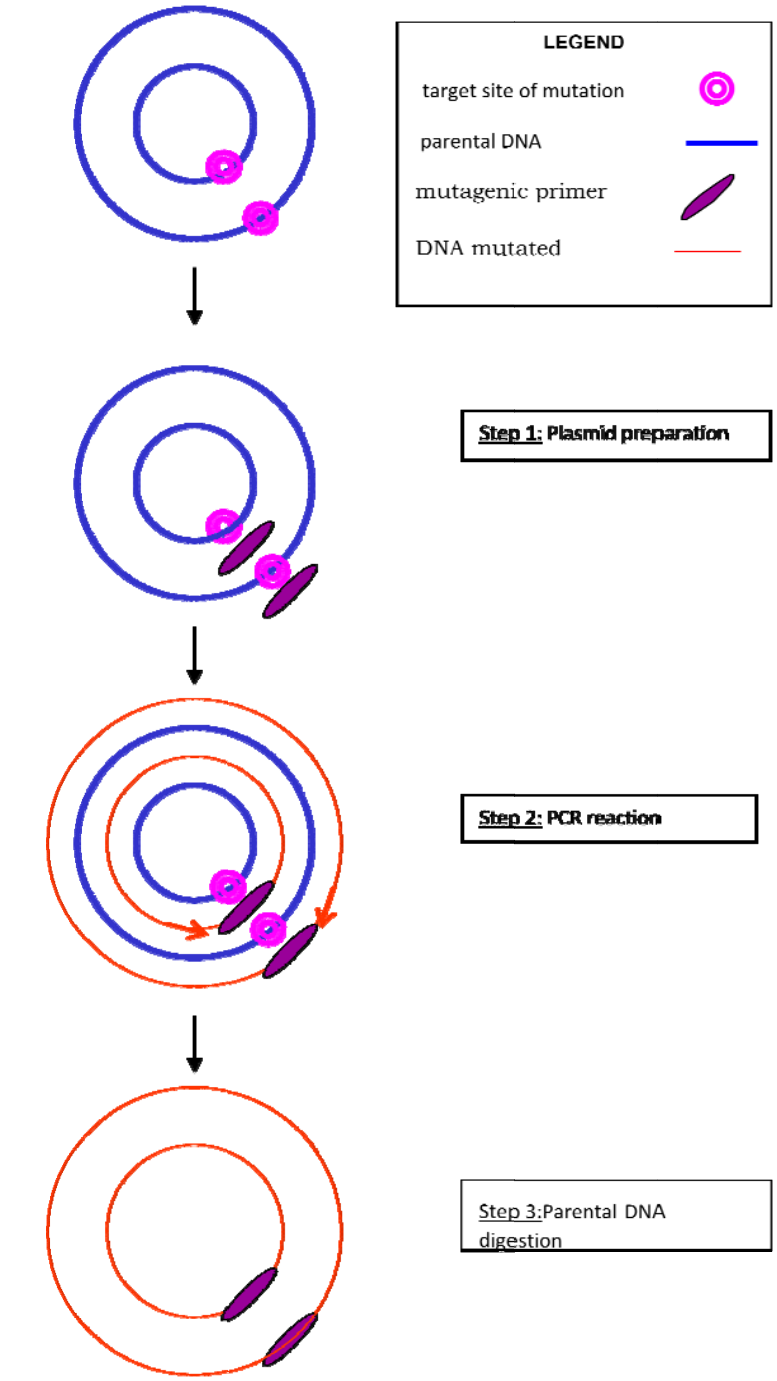

Figure 2. 4 Description of the "QuikChange Site-Directed Mutagenesis" procedure.

2.9.2 Purification of plasmidic DNA

Promega Mini Kit of Promega corporation (Madison, WI, USA) is used to purify small amounts of plasmid to transform *E. coli* strain.

PROTOCOL:

Use a single, well-isolated colony from a fresh Luria-Bertani (LB) agar plate (containing antibiotic) to inoculate 5 ml of LB medium (containing the same antibiotic).

Incubate overnight at 37°C in a shaking incubator.

Harvest bacterial culture by centrifugation for 10 minutes at 4,000 rpm in a centrifuge and discard the supernatant.

Add 250 µl of Cell Resuspension Solution and completely resuspend the cell pellet by pipetting.

Add 250 µl of Cell Lysis Solution and mix by inverting the tube 4 times and incubate for less than 5 minutes.

Add 10 µl of Alkaline Protease Solution and mix by inverting the tube 4 times. Incubate for 5 minutes at room temperature.

Add 350 µl of Neutralization Solution and immediately mix by inverting the tube 4 times.

Centrifuge the bacterial lysate at maximum speed (around 14,000 × *g*) in a microcentrifuge for 10 minutes at room temperature.

Prepare plasmid DNA purification units by inserting one Spin Column into one 2 ml Collection Tube for each sample.

Transfer the cleared lysate to the prepared Spin Column by decanting.

Centrifuge the supernatant at maximum speed in a microcentrifuge for 1 minute at room temperature. Remove the Spin Column from the tube and discard the flowthrough from the Collection Tube.

Add 750 µl of Column Wash Solution, previously diluted with 95% ethanol, to the Spin Column.

Centrifuge at maximum speed in a microcentrifuge for 1 minute at room temperature. Remove the Spin Column from the tube and discard the flowthrough.

Repeat the wash procedure using 250 µl of Column Wash Solution.

Centrifuge at maximum speed in a microcentrifuge for 2 minutes at room temperature.

Transfer the Spin Column to a new, sterile 1.5 ml microcentrifuge tube.

Elute the plasmid DNA by adding 50 µl of Nuclease-Free Water to the Spin Column. Centrifuge at maximum speed for 1 minute at room temperature.

After eluting the DNA discard the Spin Column and store the purified plasmid DNA at -20°C.

Midiprep kit of QIAGEN (Hilden, Germany) is used to obtain high amount of pure DNA to perfom site-directed mutagenesis and cloning DNA.

PROTOCOL:

Pick a single colony from a freshly streaked selective plate and inoculate a culture of 100 ml LB medium containing the appropriate selective antibiotic.

Incubate overnight at 37°C with vigorous shaking.

Harvest the bacterial cells by centrifugation at 6000 x *g* for 15 min at 4°C.

Resuspend the bacterial pellet in 4 ml Buffer P1.

Add 4 ml Buffer P2, mix thoroughly by vigorously inverting the sealed tube 4–6 times, and incubate at room temperature (15–25°C) for 5 min.

Add 4 ml of chilled Buffer P3, mix immediately and thoroughly by vigorously inverting 4–6 times, and incubate on ice for 15 min.

Clarify the lysate by filtration.

Equilibrate a QIAGEN-tip 100 by applying 4 ml of Buffer QBT, and allow the column to empty by gravity flow.

Apply the cleared lysate to the QIAGEN-tip and allow it to enter the resin by gravity flow.

Wash the QIAGEN-tip with 2 x 10 ml of Buffer QC.

Elute DNA with 5 ml of Buffer QF.

Precipitate DNA by adding 3.5 ml (0.7 volumes) of room-temperature isopropanol to the eluted DNA. Mix and centrifuge immediately at ≥15,000 x *g* for 30 min at 4°C. Carefully decant the supernatant.

Wash DNA pellet with 2 ml of room-temperature 70% ethanol, and centrifuge at ≥15,000 x *g* for 10 min. Carefully decant the supernatant without disturbing the pellet.

Air-dry the pellet for 5–10 min, and redissolve the DNA in 30 µl of molecular grade water.

Centrifuge: Eppendorf 5804 R, (Hamburg); Eppendorf 5415 (Hamburg).

2.9.3 Restriction enzyme digestion

The DNA is digested with restriction enzyme according to the method described by Sambrook *et al* (1989).

The enzymes (from Roche Diagnostics, Mannheim, Germany) are added with their respective buffers 10x concentrated. Enzymes and buffers are stored at -20°C. Digestion is performed for 1 h at 25°C and for 1 h at 37°C, adding enzymes at the beginning of digestion. The enzymes used (approximately 1U/µg of DNA) are *SmaI* (recognition sequence: CCCGGG) and *SnaBI* (recognition sequence: TACGTA). After the incubation the digestion mixture was analyzed by electrophoresis.

2.9.4 Extraction and purification of DNA fragments from agarose gel

High Pure PCR Product Purification Kit from Roche (Mannheim, Germany) is used to solubilize DNA fragments excised from agarose gel.

PROTOCOL:

Cut desired DNA band from gel using an ethanol-cleaned scalpel.

Place excised agarose gel slice in a sterile 1.5 ml microcentrifuge tube.

Determine gel mass by first pre-weighting the tube, and then reweighting the tube with the excised gel slice.

Add 300 µl Binding Buffer for every 100 mg agarose gel slice to the microcentrifuge tube.

Dissolve agarose gel slice incubating the suspension for 10 min at 56°C. Vortex the tube briefly every 2 - 3 min during incubation.

After the agarose gel slice is completely dissolved add 150 µl isopropanol for every 100 mg agarose gel slice to the tube and vortex thoroughly.

Insert one High Pure Filter Tube into one Collection Tube and pipette the entire contents of the microcentrifuge tube into the upper reservoir of the Filter Tube.

Centrifuge 30 - 60 s at maximum speed in a microcentrifuge at +15 to +25°C.

Discard the flowthrough solution and add 500 µl Wash Buffer to the upper reservoir.

Centrifuge 1 min at maximum speed and discard the flowthrough solution.

Add 200 µl Wash Buffer and centrifuge 1 min at maximum speed.

Discard the flowthrough solution and Collection Tube.

Recombine Filter Tube with a clean 1.5 ml microcentrifuge tube and add 50 - 100 µl Elution Buffer to the upper reservoir of the Filter Tube.

Centrifuge 1 min at maximum speed.The microcentrifuge tube now contains the purified DNA.

2.9.5 Ligation of DNA fragments

DNA-ligase from T4 phage is used (Roche Diagnostics, Italy) at a concentration of 1 U/µl. Plasmidic vector and linear fragment, digested with the same restriction enzymes, are combined in the appropriate buffer (66 mM Tris-HCl, 5 mM $MgCl_2$, 5 mM DTT and 1 mM ATP, pH 7.5) with 1 µl of ligase in a final volume of 30 µl. A ratio between vector and insert of 1:5 is used for the ligation, as suggested by data sheet of ligase.

Samples are incubated overnight at 16°C and then precipitated (par. 2. 4. 6) before performing the transformation.

2.9.6 DNA Precipitation

After ligation, DNA is precipitated and resuspended in distilled water to allow transformation of *E. coli* strains. The procedure is the following:

Add ethanol (2:1) and Sodium Acetate pH 5.2 at a 0.1 M final concentration.

Keep DNA at -20°C for 2h.

Centrifuge DNA at 4°C 13000 x g for 30 min. Discard the supernatant.

Wash DNA with 750 µl of cold 70% ethanol and then, centrifuge at 4°C, 13000 x g for 15 min.

Air-dry the pellet for 10 min.

Resuspend the pellet in 10 µl of sterile water.

Centrifuge: Eppendorf 5415 R, (Hamburg).

2.9.7 DNA electrophoresis

The most commonly used technique for DNA separation is horizontal electrophoresis in 0.5 to 2% agarose gels submerged in TAE buffer (TAE: solution stock 50 x: 242 g Tris base, 51.7 ml glacial CH_3COOH, 100 ml 0.5 M EDTA pH 8.0). The use of gels having different agarose concentration makes the resolution of a wide size range of DNA fragments possible. Different resolution ranges can be obtained with various concentrations of agarose.

Agarose was purchased from Sigma (Milan, Italy) in ultrapure form for molecular biology. DNA was revealed by addition of Ethidium Bromide (EtBr) to a final concentration of 0.5 μg/ml using UV excitation. To determine the sizes of the DNA "1 kb DNA Ladder" (Roche Diagnostics, Mannheim, Germany) was used. BBF-glycerol (6.2% BBF, 87% glicerol) in a 1:10 ratio with respect to the final volume, was added to the samples to prevent diffusion outside the wells and to visualize migration in the gel.

Electrophoresis was run at a constant voltage of 60 V.

Electrophoresis apparatus: Minnie Submarine Agarose Gel Unit Mod. HE 33–Hoefer (San Francisco, CA).

Power supplies: Electrophoresis Power Supply EPS 300 e EPS 1000 Pharmacia (Uppsala, Sweden); 2301 Macrodrive Power Supply – Pharmacia LKB (Uppsala, Sweden).

2.9.8 Competentation of *E. coli* for transformation with electroporation

Pick a single colony from a freshly streaked selective plate and inoculate into a culture of 5 ml LB medium containing appropriate antibiotics.

Incubate overnight at 37°C under vigorous shaking.

Add 2 ml of the cell culture to 200 ml of LB-medium containing appropriate antibiotics and incubate at 37° C under shaking until the Abs_{600} is 0.5-0.7.

- Keep cells in ice for 15-20 min.
- Centrifuge cells at 4000 x g for 15 min at 4°C.
- Resuspend the pellet in 200 ml of sterile 10% glycerol solution.
- Centrifuge cells at 4000 x g for 15 min at 4°C.
- Resuspend the pellet in 100 ml of sterile 10% glycerol solution.
- Centrifuge cells at 4000 x g for 15 min at 4°C.
- Resuspend the pellet in 4 ml of sterile 10% glycerol solution.
- Centrifuge cells at 4000 x g for 15 min at 4°C.
- Resuspend the pellet in 400 µl of sterile 10% glycerol solution.
- Store cells in aliquots at -80°C for at last 6 months.

Centrifuge: Eppendorf 5804 R,(Hamburg).

2.9.9 Transformation of *E. coli* by electroporation

- Thaw in ice an aliquot of the competent cells for each transformation.
- Put the electroporation chambers in ice.
- Pipet 5-10 µl of each ligation mixture into the cells suspension and mix gently. Incubate in ice for 10 min.
- Transfer cells into the electroporation chamber.
- Set the electroporation apparatus to 750 V and apply an electrical discharge.
- Add 1 ml of sterile medium and leave cells at 37°C for 1 h.
- Centrifuge at 4000 x g for 15 min at 4°C.
- Discard the supernatant.
- Resusped cells in 200 µl of LB medium.
- Plate on LB plate with appropriate antibiotics at 1/10 and 9/10 diluitions.
- Incubate overnight at 37°C.

The following day some colonies grow on the plate.

Electroporator: Bio-Rad model 1000/500 power supply; electroporator: elettroporator Co_Co.

Centrifuge: Eppendorf 5804 R,(Hamburg).

2.10 Synthesis of radioactive RNA

2.10.1 Plasmid used

The radioactive, 375-nt transcript from the *malE-malF* intergenic region RNA (MALEF probe) was synthesized as described (McLaren *et al*., 1991; Causton *et al*., 1994) using the plasmid pGM923.2 derivated from plasmid pGEM®-4Z digested with KpnI e BamHI.

2.10.2 Riboprobes used

malEF: obtained by transcription *in vitro* with T7 phage RNA polymerase of pGM923.2 digested with EcoRI.

Table 2.5. Oligonucleotides:

Code[a]	Sequence 5'-3'	Complementary region	Tm
FG1581/30	AAA GGT ACC CCA TGG GGT TCT TCC TCA TTC[c]	Intergenic region *malEF* of *E.coli*	68,1° C [59°C][b]
FG1582/31	AAA GGA TCC CCA TGG AAA ACG CCC AGA AAG[c]	Intergenic region *malEF* of *E.coli*	68,1° C [59°C] [b]
FG1586/20	ACG ACG GCC AGT GAA TTG GA		59,4° C
FG1587/20	CAC TTT ATG CTT CCG GCT CG		59,4° C

[a] The number after the slash (/) shows the oligo length in nucleotides.
[b] The number indicated between the two parentheses corresponds to the Tm of the oligo without tail.
[c] In block letter are indicated the sequences of the situated ones of restriction.

2.11 Functional assay of degradosome

2.11.1 Reaction mixture

Tris-HCl	20 mM
DTT	1.5 mM
Magnesium acetate	1 mM
KCl	20 mM
K_2HPO_4	10 mM

Where indicated ATP was added 1 mM final.

2.11.2 Functional assay

The RNA (10 ng; 1 *10^5 c. p. m.) was incubated with 0.16 μg degradosome at 26° C in a final reaction volume of 30 μl containing the reaction mix described.

Samples (4 μl) were withdrawn before (time 0), and 0, 5, 15, 30 and 60 min after addition of enzyme. The reaction was stopped by additing 9 μl of a formamide-dye loading mix, and 4 μl was then electrophoresed on a 6% sequencing gel.

2.12 Degradation and 3'-tailing of PNPL1 RNA

For degradation and polymerization assays with a specific RNA substrate, 32P-labelled PNPL1 RNA was synthesized by in vitro transcription with T7 RNA polymerase and [α-32P]CTP using a DNA template obtained by PCR amplification of plasmid pAZ101 (11) with oligonucleotides FG676(5'-ctaatacgactcactatagggATGAATGATCT TCCGTTGC; lower case letters, T7 promoter; uppercase letters, *E. coli*) and FG1387(5'-

AATGTAATATCCTTTCTCTTTCTT AG). PNPL1 RNA encompasses the first 158 nt of the non-processed pnp transcript from the pnp-p promoter.

Phosphorolysis was performed at 26 °C in 30 µl reaction buffer (10 mM Tris HCl, pH 7.4; 0.75 mM DTT; 4.5 mM Mg acetate; 10 mM KCl) containing 0.2 µM PNPL1 (35000 cpm), 8.6 nM PNPase, and 10 mM Pi. Polymerization was performed in the same conditions with 1 mM ADP and omitting Pi. Reactions were stopped by adding 3 µl samples to 5 µl stop solution (95% formamide, 20 mM EDTA, 0.05% bromophenol blue, 0.02% xylene cyanol) and heating for 5 min at 95 °C. The samples were analysed by denaturing 6% acrylamide gel electrophoresis and the autoradiographic image was acquired by phosphorimaging the exsiccated gel.

2.13 Cross-linking of ATP with PNPase

14 pmoles of wt or His-tagged PNPase were incubated 10 min at room temperature with 20 µCi of [α-^{32}P]ATP (3000 Ci/mmol) in 50 mM Tris-HCl pH 7.5, 8 mM $MgCl_2$ 0.4 mM DTT (total volume of 30 µl). 10 µl droplets of the samples on parafilm were UV-irradiated at 254 nm in a Stratalinker (Stratagene) for different times . After the addition of one volume of 2x SDS-loading buffer (100mM Tris-HCl pH 6.8, 200 mM DTT, 4% SDS, 0.2% bromophenol blue, 20% glycerol), the samples were boiled for 3 min and loaded on a 10% polyacrylamide denaturing gel.

2.14 Molecular docking

The molecular docking is a computational technique to predict very carefully the structure of the complex between two interacting molecules, tipically a protein with a ligand (Goodford, 1985). This is an helpful technique to understand the mechanism whereby a protein binds substrate or any cofactors. In any docking scheme two conflicting requirements must

be balanced: the desire for a robust and accurate procedure, and the desire to keep the computational demands at a reasonable level. The ideal procedure would find the global minimum in the interaction energy between the substrate and the target protein, exploring all available degrees of freedom for the system.

We used two different computational programs: moe and Autodock 4.

2.14.1 MOE 2002.03 (Molecular Operating Environment)

Docking simulations were performed using the software MOE because it provides a wide range of options for creating, assembling and modifying molecules. This application also allows to conduct docking calculations and molecular dynamics.

In our studies we utilized a PNPase dimer, thus making the system less complex and ensuring shorter computing times. For this purpose, we constructed the dimer from the monomer crystallographic structure, downloaded from the *Protein Data Bank.* Using the function *Add Hydrogens*, we added the hydrogen atoms, not present in the protein data bank file to both potein and ATP. Water molecules were not taken into account in computing. The option S*ite Finder* was used to identify possible ATP binding sites by docking analysis.

2.14.2 Autodock 4

Autodock 4 (http://autodock.scripps.edu) is a free software to calculate binding energy between protein and ligand.

Rapid energy evaluation is achieved by precalculating atomic affinity potentials for each atom type in the substrate molecule in the manner described by Goodford (Goodford, 1985). In the **AutoGrid** procedure the protein is embedded in a three-dimensional grid and a probe atom is placed at each grid point.

The energy of interaction of this single atom with the protein is assigned to the grid point. An affinity grid is calculated for each type of atom in the substrate, typically carbon, oxygen, nitrose and hydrogen, as well as a grid of electrostatic potential, either using a point charge of +1 as the probe, or using a Poisson-Boltzmann finite difference method, such as DELPHI 2.3. The energetics of a particular substrate configuration is then found by tri-linear interpolation of affinity values of the eight grid points surrounding each of the atoms in the substrate. The electrostatic interaction is evaluated similarly, by interpolating the values of the electrostatic potential and multiplying by the charge on the atom (the electrostatic term is evaluated separately to allow finer control of the substrate atomic charges). The energy calculation using the grids is proportional only to the number of atoms in the substrate, and not to any function of the number of atoms in the protein.

The docking simulation is carried out using the *Metropolis method*, also known as *Monte Carlo simulated annealing*. With the protein static throughout the simulation, the substrate molecule performs a random walk in the space around the protein. At each step in the simulation, a small random displacement is applied to each of the degrees of freedom of the substrate: translation of its center of gravity; orientation; and rotation around each of its flexible internal dihedral angles. This displacement results in a new configuration, whose energy is evaluated using the grid interpolation procedure described above. This new energy is compared to

the energy of the preceding step. If the new energy is lower, the new configuration is immediately accepted. If the new Energy is higher, then the configuration is accepted or rejected based upon a probability expression dependent on a user defined temperature, *T*. The probability of acceptance is given by:

$$P(\Delta E) = e^{\left(-\frac{\Delta E}{k_B T}\right)}$$

where D*E* is the difference in energy from the previous step, and *kB* is the Boltzmann constant. At high enough temperatures, almost all steps are accepted. At lower temperatures, fewer high energy structures are accepted.

The simulation proceeds as a series of cycles, each at a specified temperature. Each cycle contains a large number of individual steps, accepting or rejecting the steps based upon the current temperature.

After a specified number of acceptances or rejections, the next cycle begins with a temperature lowered by a specified schedule such as:

$$T_i = gT_{i-1}$$

where *Ti* is the temperature at cycle *i*, and *g* is a constant between 0 and 1. Simulated annealing allows an efficient exploration of the complex configurational space with multiple minima that is typical of a docking problem. The separation of the calculation of the molecular affinity grids from the docking simulation provides a modularity to the procedure, allowing the exploration of a range of representations of molecular interactions, from constant dielectrics to finite difference methods and from standard 12-6 potential functions to distributions based on observed binding sites.

3. RESULTS

3.1 ATP inhibits RNA degradosome activity

While performing functional assays with RNA degradosomes assembled with mutant PNPases isolated in our laboratory (Briani et al. 2007), we observed that ATP concentrations higher than 5 mM retarded the appearance of degradation products (Fig. 3.1).

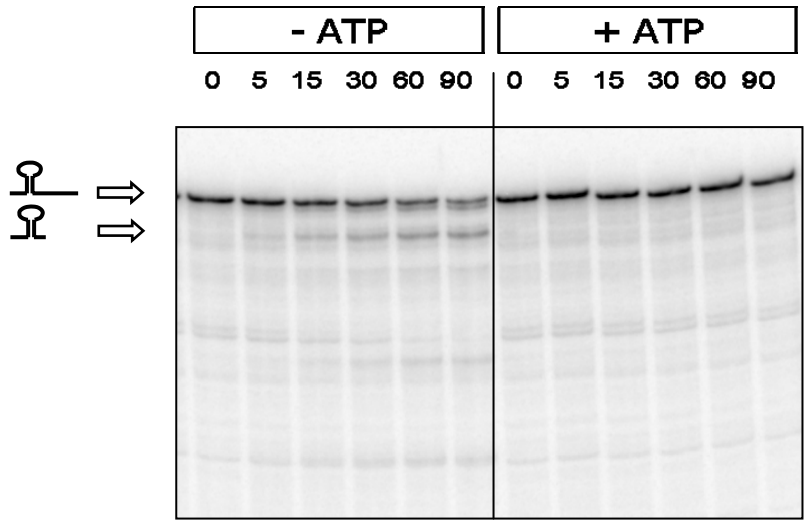

Figure 3.1. Degradation profile of the MALEF riboprobe by Pnp-E81K mutant degradosome. Purified Pnp-E81K RNA degradosome (0.04 µg) was incubated for the indicated times (min) with 10 ng of 32P labelled malE-malF riboprobe in 30 µl of 20 mM Tris-HCl, pH 7.5, 1.5 mM DTT, 1mM Mg acetate, 20 mM KCl, 10 mM K2HPO4; at 26°C in the presence or in the absence of ATP.

3.2 ATP inhibits both PNPase enzyme activities

To discriminate whether ATP directly inhibits the catalytic activity of PNPase rather than other properties of the entire degradosome, we tested the effect of ATP on purified PNPase by monitoring shortening and

elongation of a specific RNA (PNPL1) substrate in presence of phosphate and ADP, respectively. PNPL1 is predicted to form a long stable stem-loop at the 5'-end, followed by a less structured 3'-tail (Fig. 3.2).

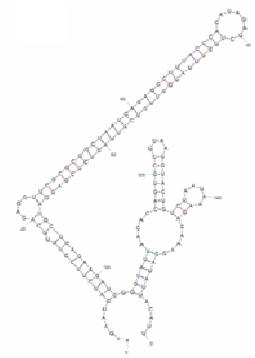

Figure 3.2. Secondary structure of PNPL1 RNA computed using Mfold (Zuker 2003) showing a 99-nucleotide-long hairpin structure at the 5'-end and a looser conformation of the 3'-region. The two bases preceding the 5'-end of *pnp-p* RNA are *lowercase.*

As shown in Fig. 3.3 , incubation of ^{32}P-labeled PNPL1 with PNPase in the presence of phosphate led to the accumulation of an ~ 100-nucleotide-long degradation product, whereas the same substrate in the presence of ADP was elongated up to ~ 1 kb after a 30 min incubation. Both phosphorolysis and polymerization were, however, completely inhibited by 10 mM ATP.

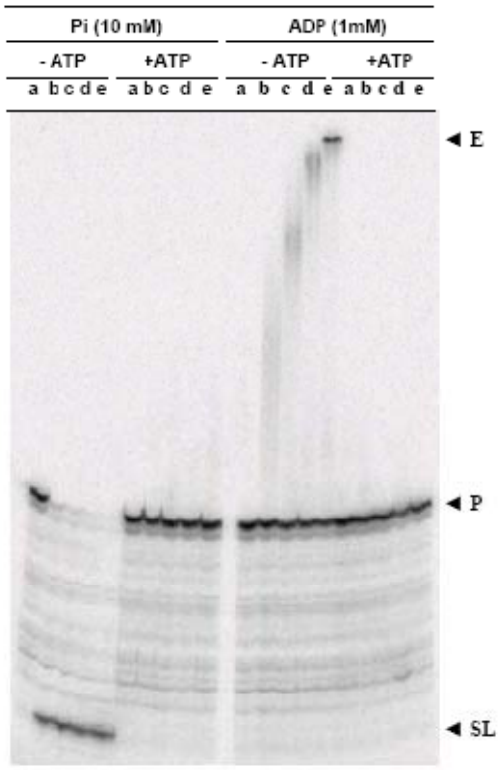

Figure 3.3 Degradation (10 mM phosphate) and polymerization (1 mM ADP) reactions with or without 10 mM ATP. Lanes a-e, reaction times of 0, 2.5, 5, 10, and 30 min, respectively. The arrowheads point to PNPL1 (P) and the ~ 100-base-long stem-loop degradation (SL) and ~ 1-kb-long elongation (E) products.

To rule out that phosphate and ADP, which are spontaneous ATP hydrolysis products, could be responsible for these inhibitory effects by driving in the opposite direction the reversible reactions, we performed the PNPase assay in 1 mM ADP and varying phosphate concentrations. As show in Fig 3.4/A, phosphate up to 0.3 mM did not reverse the polymerization reaction with 1 mM ADP, whereas 1 mM ADP did not reverse the polymerization reaction with 10 mM phosphate. Thus, contamination of phosphate and ADP up to 3 and 10 %, respectively, of the ATP concentration used in the previous experiment would be not be influential on the PNPase reactions. By varying the ATP concentration, we observed

that, under our assay conditions, 4 mM ATP substantially inhibited both phosphorolytic and polymerizing activities (Fig. 3.4A and B).

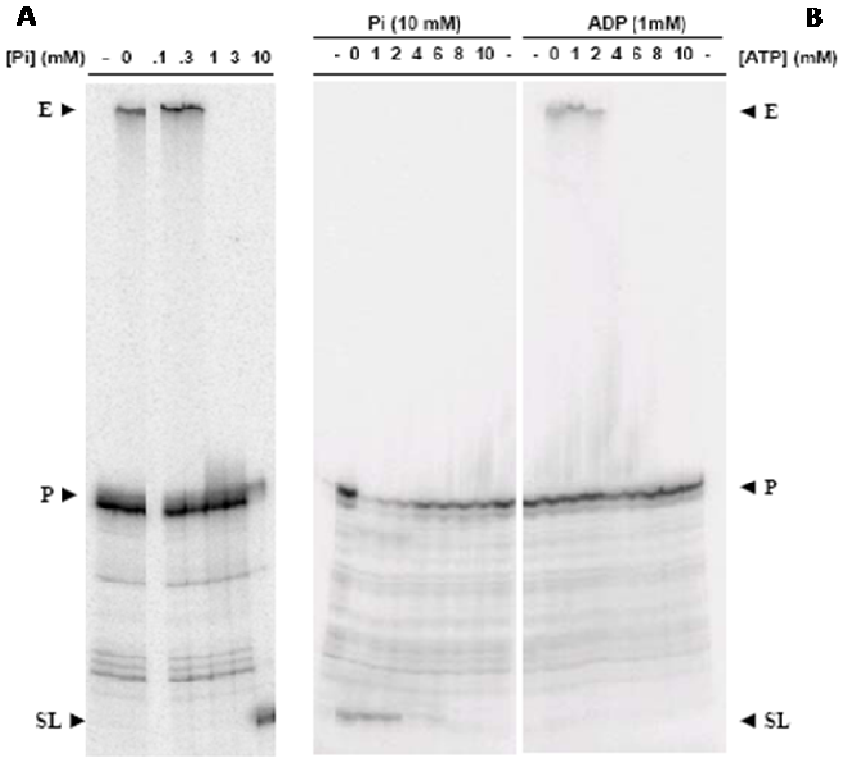

Figure 3.4 PNPase inhibition by ATP. A) polymerization reaction performed in the presence of 1 mM ADP and increasing phosphate concentrations and quenched after 30 min. -, no PNPase added. B) degradation (10 mM phosphate) and polymerization (1 mM ADP) reactions at increasing ATP concentrations. The arrowheads point to PNPL1 (P) and the ~ 100-base-long stem-loop degradation (SL) and ~ 1-kb-long elongation (E) products.

3.3 PNPase binds ATP

To test whether PNPase can directly bind ATP, we performed affinity labeling experiments by UV cross-linking radiolabeled ATP to PNPase. As shown in Fig. 3.5A, both [α-32P]ATP and [γ-32P]ATP (0.33 μM) were cross-linked to PNPase. This indicates that ATP, rather than its spontaneous hydrolysis product ADP, AMP, or phosphate, was cross-linked to PNPase.

No cross-linking could be detected with carboxypeptidase used as a control, whereas a weak signal (barely visible in the original scan) in the absence of MgCl2 was detectable with ribosomal protein S1. 10 mM MgCl2 reduced but did not abolish cross-linking. Affinity labeling was not competed by 33 µM ADP.

Interestingly, however, cross-linking was essentially not competed by unlabeled ATP up to ~ 100 µM (Fig. 3.5, B and C) thus suggesting that 0.33 µM ATP was far from saturation, in keeping with the I0.5 values determined for the nucleotide (see below).

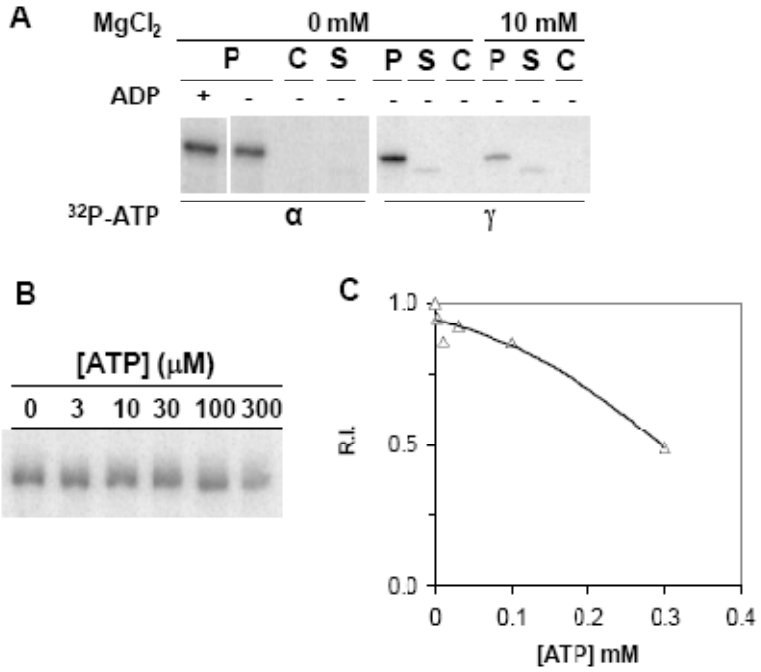

Figure 3.5 Affinity labeling of PNPase by UV cross-linking with [^{32}P]ATP. A) 2 pmol of PNPase (P), bovine pancreas carboxypeptidase (C), or *E. coli* His-tagged ribosomal protein S1 (S) was incubated in 10 µl reaction mixtures with 0 or 10 mM $MgCl_2$ and 3.3 pmol of either [α^{32}P]ATP or [γ^{32}P]ATP as indicated. In one sample, 33 µM ADP was also added. B) 2 pmol of PNPase was incubated in 10 µl reaction mixtures with 3 pmol of [α^{32}P]ATP and unlabeled ATP at the concentrations indicated. C) the relative intensity (R.I.) of the signals in B was plotted against the unlabeled ATP concentration.

3.4 ATP allosterically inhibits PNPase

To perform kinetic analysis of PNPase phosphorolytic activity at different ATP concentrations, we used polyA as a substrate and measured the appearance of ADP in a coupled pyruvate kinase/lactate dehydrogenase assay at constant saturating polyA (30 μg/ml) and at varying phosphate concentrations. The results (Fig. 3.6A) were consistent with a mixed-type inhibition (Segel, 1975), with a scanty increase in K_m and a substantial decrease in V_{max} upon increasing ATP concentrations. Thus, the pattern observed is close to pure noncompetitive inhibition. In particular, V_{max} dropped from ~ 0.7 to 0.2 units/mg when ATP was raised from 0 to 5 mM. Similar results were obtained at fixed phosphate and varying polyA concentrations. However, at polyA concentrations close to or lower than K_m (~ 1 μg/ml), measurements were subject to a large dispersions, which prevented us from accurately determining the kinetic parameters. In any case, the activity was completely abolished even at 30 μg/ml polyA, thus ruling out competitive inhibition. We therefore conclude that the ATP-binding site is distinct from that of both substrates.

According to the kinetic model, replots of slopes and 1/v axis intercepts as a function of inhibitor concentration should yield straight lines with intercepts on the abscissa that equal the inhibition constant (Segel, 1975). However, following this procedure, we surprisingly observed large and systematic deviations from linearity of the experimental points. We thus conclude that PNPase does not conform to a classical mixed-type or noncompetitive inhibition model. Moreover, when plotting the percentage of PNPase inhibition *versus* ATP concentration at saturating substrates, a sigmoidal curve was obtained (Fig. 3.6B) which clearly points to cooperative allosteric binding of the nucleotide. Based on the best fitting curve, a Hill coefficient of 2.3 and an $\boldsymbol{I}_{0.5}$ (i.e. a concentration that gives 50% inhibition)

of 3.3 mM were estimated. The experiments were performed at 5 and 13 mM $MgCl_2$, and the results obtained under either condition were superimposable (Fig 3.6B). This rules out the hypothesis that the inhibition observed depends simply on depletion of Mg^{2+} (an ion required for PNPase activity) complexed with ATP. A similar profile was obtained with purified FLAG-Rne degradosome rather than trimeric PNPase (data not shown).

To detect the effect of ATP in the synthetic direction, we measured the released phosphate using a commercially available enzymatic kit assay for phosphate detection that allows continuous measurements of PNPase activity. The data shown in Fig. 3.6C indicate that ATP also inhibits polymerization at both 5 and 13 mM $MgCl_2$ with $I_{0.5}$ values of ~ 5 mM.

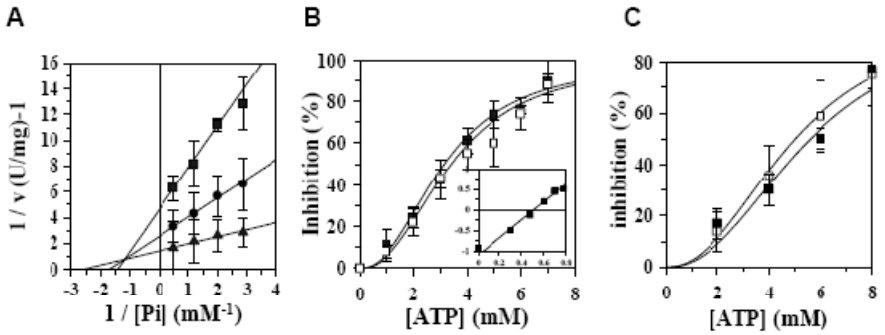

Figure 3.6 Kinetic analysis of PNPase inhibition by ATP. A) Double reciprocal plots of PNPase phosphorolytic activity at varying phosphate concentrations. The activity was assayed at 28°C as described under Materials and methods, 2.7.1. ATP concentrations were 0 mM (▲), 2 mM (●), and 5 mM (■). Each point is the mean of at least four independent determinations. Vertical bars represent standard deviations. B) Inhibitory effect of ATP towards PNPase phosphorolytic activity. The activity was assayed at 28°C in the presence of 30 μg/ml poly(A), 10 mM phosphate and either 5 (open symbols) or 13 mM MgCl2 (closed symbols). Inhibition is expressed as percentage of the samples without ATP. Each point is the mean of at least four independent determinations. Vertical bars represent standard deviations. Inset: Hill plot of the ATP inhibitory effect. Abscissa: log[ATP]; ordinate: log(f/1-f), where f represents the fraction inhibited. C) Inhibitory effect of ATP towards PNPase synthetic activity. The activity was assayed at 25°C in the presence of 0.2 mM ADP, 20 μg/ml poly(A) and either 5 (open symbols) or 13 mM $MgCl_2$ (closed symbols). Each point is the mean of at least four independent determinations. Vertical bars represent standard deviations.

3.5 Effect of other nucleoside triphosphates on PNPase

We also checked the effect of other nucleoside triphosphates on PNPase activity. Our results show that purine nucleotides GTP, dGTP, dATP, and non-hydrolyzable ATP were also inhibitory, whereas the pyrimidine nucleotides CTP and UTP did not exert any appreciable effect (Tab. 3.1).

Table 3.1 Inhibitory effect of different nucleoside triphosphates on PNPase phosphorolytic activity.
Assays were performed at 28°C as described under (Materials and methods, 2.7.1) in the presence of the nucleotide to be tested (5 mM) and MgCl2 (13 mM).

	ATP	**dATP**	**β,γ-imido-ATP**	**GTP**	**dGTP**	**CTP**	**UTP**
Residual activity (%)[a]	30	39	50	65	40	102	98

[a] The activity (average of at least three independent measurements) is expressed as a percentage of the control assays without nucleotide added.

3.6 Molecular Modeling of the ATP-binding site

In order to identify the ATP-binding site(s) of PNPase, we performed a modeling analysis. Initially we identified properties shared by ATP-binding sites in a protein database. This preliminary analysis lead to define two typical features for this interaction: one is the presence of the basic residues arginine and lysine, that bind the phosphate residues; another is the presence of hydrophobic amino acids, in particular tryptophan and phenylalanine, that bind to adenine. Then, we used the MOE program (Materials and Methods 2.12.1) and in particular the function “site finder”

to spot such sites. This lead to the identification of two putative sites (Fig. 3.7).

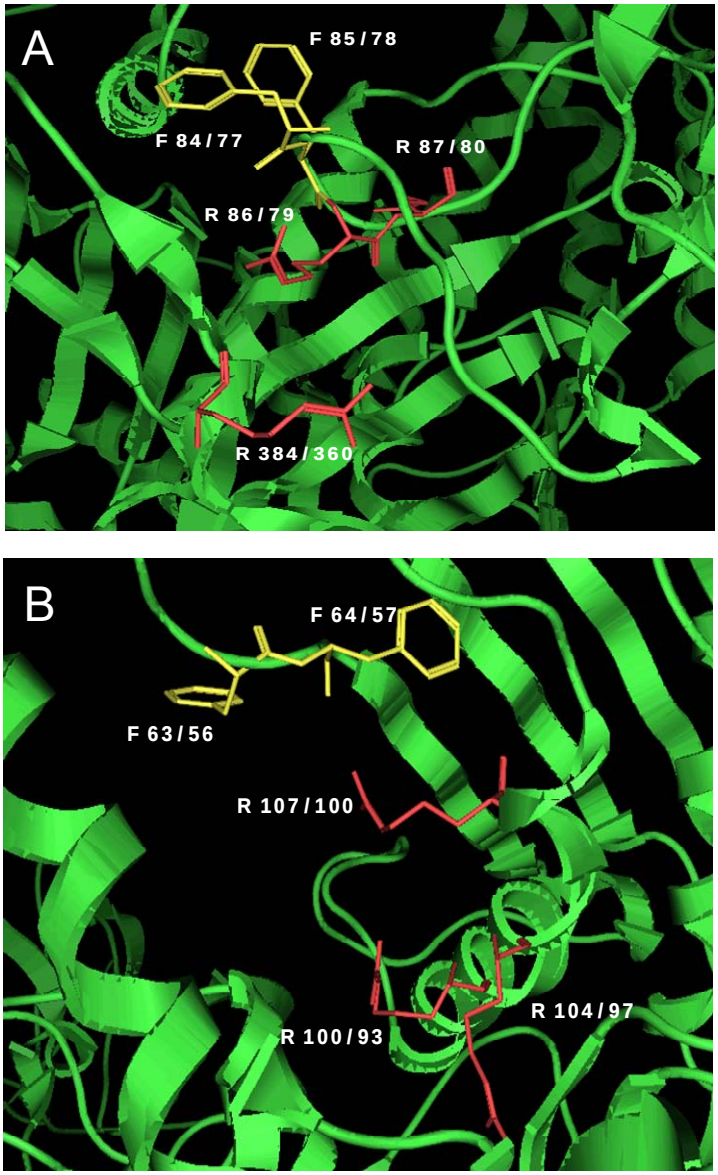

Figure 3.7 Computational model of the two putative ATP-binding sites on PNPase identified with the MOE program. The residues are labeled with double numeration: the first corresponds to the residue numbering in *S. antibioticus*; the second to the *E. coli* residue numbering.

In the *E. coli* enzyme, one site consists of the following five residues: Phe77, Phe78, Arg79, Arg80 and Arg360 (fig. 3.7A); in the other the residues are Phe56, Phe57, Arg93, Arg97 and Arg100 (Fig. 3.7B).

These results suggest therefore a strategy for further mutational analysis aimed at characterizing different mutations of the above residues with regard to their effects on PNP activity and ATP inhibition.

3.7 Production and analysis of PNPase mutants

We replaced by alanine the residues identified by the modeling analysis, thus producing the PNPase mutants: F77A, F78A, R79A, F56A, R93A, F103A. Then, we checked the effect of these mutations on ATP inhibition. Tab. 3.2 shows the percentage of residual activity in the mutants in the presence of 4 or 8 mM ATP with respect to the wt all mutants were inhibited. In particular, at 8 mM ATP the nucleotide completely abolished the activity.

Table 3.2. ATP inhibition of PNPase mutants

Strain	Mutant	Residual activity (%) with respect to wt	
		4 mM ATP	8 mM ATP
	wt	50	b.d. [a]
1101	F77A	46	b.d. [a]
1102	F78A	53	b.d. [a]
1103	R79A	45	b.d. [a]
1104	F56A	67	b.d. [a]
1105	R93A	b.d. [a]	b.d. [a]
1106	F103A	34	b.d. [a]

[a] below detection limit.

We also observed that the mutant F103A displayed an activity significantly lower than the wt, and the mutant R93A was completely inactive. Furthermore, even the polymerase activity of these mutants was similarly reduced and, in addition, F77A and R79A also were significantly less active than the wt (Tab. 3.3). These findings suggest that all of the aforementioned mutants may be in some way involved in PNPase catalysis.

Table 3.3. Polymerization activity of PNPase wt and mutants

Strain	Mutant	Residual activity (%) respect to wt
wt	wt	100
1101	F77A	19
1102	F78A	76
1103	R79A	2
1104	F56A	76
1105	R93A	b.d. [a]
1106	F103A	26

[a] below detection

3.8 Biochemical characterization of PNPase mutants

Based on the aforementioned results, we undertook a kinetic characterization of some mutants impaired in catalytic activity. In particular, we focused on F77A and R79A, as they are reported to be located in the FFRR loop that has been suggested to be involved in RNA binding (Regonesi, 2004).

We determined the kinetic parameters both in the synthetic and the phsphorolytic directions (Table 3.4; some representative Michaelis/Menten profiles are shown in fig 3.8 and 3.9).

Table. 3.4. Kinetic parameters in the synthetic and the phosphorolytic directions. For further details see Materials and Methods 2.7.2.

	Synthesis		**Phosphorolysis**			
	ADP		P_i		polyA	
	K_m	k_{cat}	K_m	k_{cat}	K_m	k_{cat}
wt	0.1	30	0.27	106	0.9	89
F77A	0.02	18	0.34	67	0.6	54
R79A	3.7	69	4	111	0.4	46

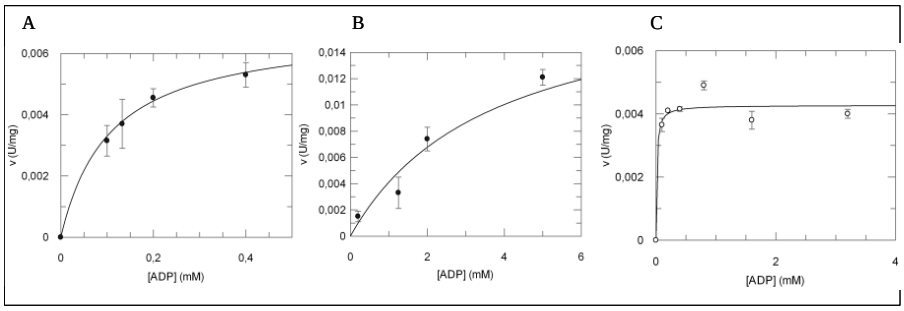

Figure 3.8. Reaction velocity profiles as a function of ADP concentration (mM) of PNPase wt (A), R79A (B), F77A (C). The activity was assayed at varying ADP concentrations, in the presence of 20 µg/ml poly(A). Each point is the mean of at least three independent measurements. Vertical bars represent standard deviations.

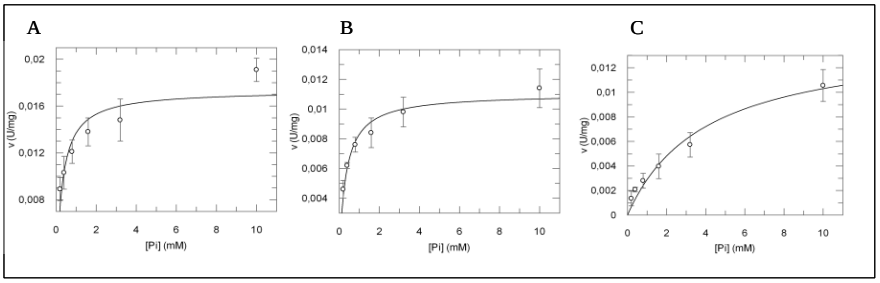

Figure 3.9. Reaction velocity profiles as a function of phosphate concentration (mM) of PNPase wt (A), F77A (B), R79A (C). The activity was assayed at varying phosphate concentrations, in the presence of 30 µg/ml poly(A). Each point is the mean of at least three independent measurements. Vertical bars represent standard deviations.

Our result show, first of all, that the mutagenized residues cannot be involved in the catalytic step; otherwise, their replacement by alanine

should result in a dramatic k_{cat} reduction. Small variations may be accounted for by conformational changes induced by the mutations. Likewise, the K_m values for polyA did not vary significantly among the three enzyme forms, suggestive of the fact that the mutated residues do not participate in RNA binding.

As regards the effect of the R79A mutation on the K_m values for ADP and phosphate, it is apparent a strong increase (20-40-fold) for both substrates: this points to an involvement of Arg79 in binding of both free phosphate and the terminal ADP phosphate. No such effect was observed for F77A, which suggests that Phe77 does not play a role in the overall catalytic process.

3.9 Docking studies on Streptomyces antibioticus PNPase

We than conducted a docking study to assess to mode of ADP binding by the residue Arg79. We used Autodock 4; a program specifically developed for predicting the interaction of small molecules with macromolecular target (Materials and methods 2.12.2) .

As a model to start with docking studies we used S. antibioticus GPSI/PNPase crystal structure because was the only referenced structure available during our studies. This protein has a high percentage of identity (47%) with E. coli PNPase.

In the first experiment using Autodock 4 and utilizing the option to maintain flexible residues Arg79, Arg80 and Arg83 (Arg86, Arg87 and Arg90 in S. antibioticus) we identified a putative ADP-binding site close to the residue Arg79. We created a 60 x 60 x 60 Å grid centered on flexible residues of a monomer of PNPase. The program uses Monte Carlo-

simulated annealing to explore a wide range of conformational states. A "job" consists of a number of independent runs, each of which begins with the same initial conditions. During each cycle, random changes are made to the ligand's current position, orientation, and conformation if flexibiliy was defined. The resulting new state is then compared to its predecessor; if the new energy is lower than the last, this new state is accepted. The user can select the minimum energy state found during a cycle to be used as the initial state for the next cycle, or the last state can be used. The best results tend to be achieved by selecting the minimum energy state from the previous cycle. When more than one run is carried out in a given job, cluster analysis or 'structure binning' will be performed, based on structural rms difference, ranking the resulting families of docked conformations in order of increasing energy.

Results are shown in tab. 3.5. We obtained 9 clusters and the relevant binding energies and dissociation constants.

Table 3.5. Computational clusters of PNPase wt-ADP structures and the rlevant binding energies.

Cluster	Binding energy (kcal/mol)	K_d
1_1	-13.88	66.95 pM
2_1	-13.71	89.24 pM
3_1	-13.37	158.00 pM
4_1	-12.90	348.18 pM
5_1	-12.61	575.74 pM
6_1	-12.19	1.16 nM
6_2	-11.99	1.63nM
7_1	-11.59	3.2 nM
8_1	-11.18	6.42 nM

9_1	-10.87	10.75 nM

In the binding model shown in fig. 3.10, Arg90, Phe84 and Phe85 (Arg83, Phe77 and Phe78 in *E. coli*) make hydrogen bonds with ADP. Unexpectedly, in no docking structure was a direct interaction between ADP and *E. coli* Arg79 highlighted, as instead suggested by our experimental results.

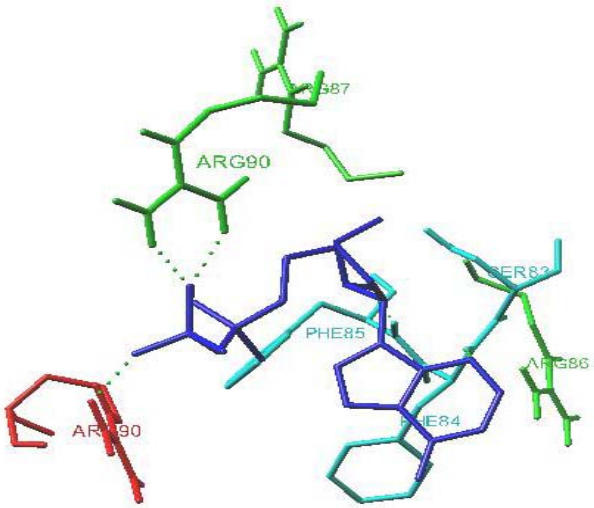

Figure 3.10 Lowest energy conformation of PNPase with ADP (-13.88 kcal/mol; K_d 66.95 pM). Blue: ADP, green: flexible residues, red: monomer A inflexible residues , light blue: monomer B inflexible residues. Hydrogen bonds: Arg90 (monomer B): 2; Arg90 (monomer A): 1; Phe84 (monomer B): 1; Phe85 (monomer B): 1.

To evaluate the possible role of this residue in the ADP-binding we conducted another docking analysis using a PNPase variant carrying the R79A mutation (R86A in *S. antibioticus*). As flexible residues were selected Arg87, Arg90 (Arg80, Arg83 in *E. coli*). We obtained 8 conformational clusters (tab. 3.6). The lowest energy structure is reported in fig. 3.11.

Table 3.6. Computational clusters of PNPase R79A-ADP structures and relevant binding energies.

Cluster	Binding Energy (kcal/mol)	K_d
1_1	-10.05	43.29 nM
1_2	-9.08	220.24 nM
2_1	-9.81	64.29 nM
2_2	-9.56	97.97 nM
3_1	-9.72	75.56 nM
4_1	-9.54	102.48 nM
5_1	-9.34	143.61 nM
6_1	-8.52	567.06 nM
7_1	-8.51	575.93 nM
8_1	-8.26	888.29 nM

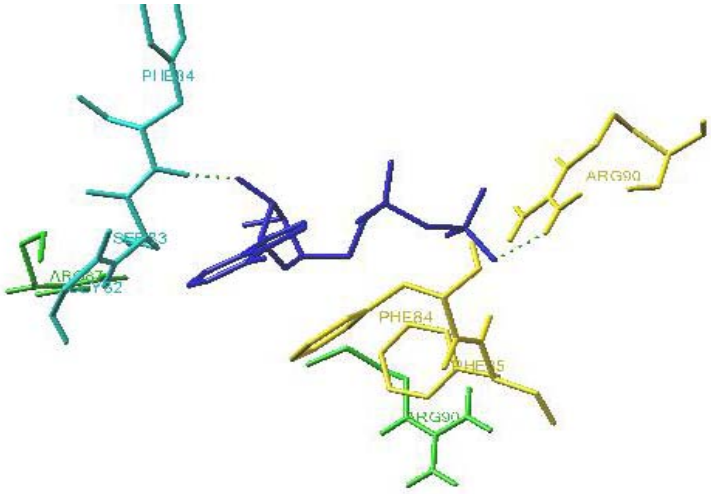

Figure 3.11. Lowest energy conformation of PNPase R79A with ADP (-10.05 kcal/mol; K_d 43.29 nM). Blue: ADP, green: flexible residues, red: monomer A inflexible residues , light blue: monomer B inflexible residues. Hydrogen bonds: Arg90 (monomer C): 1; Phe84 (monomer B): 1; Phe85.

These data show that the R79A PNPase has a much lower affinity and binding energy than the wt. These results confirm the involvement of Arg79 in the ADP-binding, thus suggesting an indirect interaction, for instance through long range electrostatic interactions. Alternatively this residue may have a structural role in substrate recruitment.

3.10 Production and analysis of PNPase mutants to investigate substrate-binding site

Following our biochemical and docking analysis, we extended our investigations by producing and characterizing further mutants. We produced R83A as our docking experiments (see previous par. 1.9) suggest its involvement in ADP binding. Furthermore, a paper published during this work (Shi *et al.* 2008) suggests a role for Arg80 in RNA binding. This prompted us to also produce R80A and R79A/R80A mutants. Then, we determined their kinetic parameters, both in the synthetic and the phosphorolytic directions (Table 3.7).

We first observed that the activity of the double mutant was so dramatically impaired that this prevented us from performing any kinetic measurement. As regards the other mutants, i.e., R80A and R83A, both their k_{cat} and K_m for polyA were not very much different from that of the wt, similar to the case of F77A and R79A. This shows that the mutagenized residues are not involved in the catalytic step, nor do they apparently participate in RNA binding.

Table. 3.7. Kinetic parameters in the synthetic and the phosphorolytic directions. For further details see Materials and Methods 2.7.2.

	synthesis		**phosphorolysis**			
	ADP		P_i		polyA	
	K_m	k_{cat}	K_m	k_{cat}	K_m	k_{cat}
wt	0.1	30	0.3	106	0.91	89.1
R80A	12	75.6	5.9	51.9	1.35	77.5
R83A	0.02	48.3	1.7	68.4	0.98	70.8
R79A/R80A	b.d.[a]	b.d.[a]	b.d.[a]	b.d.[a]	b.d.[a]	b.d.[a]

[a] below detection

With regard to the K_m for ADP and phosphate, R80A behaved quite similar to R79A, suggestive of a role in free phosphate and ADP terminal phosphate binding. Rather puzzling was instead the behavior of R83A that displayed an increased K_m for phosphate and a decreased one for ADP. In our opinion, this is not representative of an involvement of Arg83 in ADP/phosphate binding, as this should plausibly result in similar changes in K_m for either substrates. Probably, the detected pattern may be due to conformational changes close to, or in the nucleotide-binding site.

In conclusion, so far our investigations make it possible to conclude that the residues Arg79 and Arg80, located in the FFRR loop, participate in ADP/phosphate binding but not in RNA binding.

4. DISCUSSION

mRNA levels are subject to transcriptional and post-transcriptional control. This allows rapid changes in the levels of individual mRNA species in response to defined intracellular signals. In *Escherichia coli*, the overall pathway for mRNA degradation is well established (Coburn and Mackie, 1999), although much remains to be learned about its control in this different pathway and under conditions of stress or shock. In all three domains of life – Bacteria, Archaea and Eukarya – the machinery of RNA degradation often takes the form of multicomponent assemblies, and these complexes, or their individual components, can target specific gene products or affect the relative composition of different transcripts through differential decay rates (Carpousis *et al.*, 2002). From the perspective of regulatory control networks, RNA degradative machines effectively function as trans-acting regulators of gene expression, similar to the classical transcription factors that control rates of mRNA synthesis.

In the well-studied bacterium *Escherichia coli*, a multi-enzyme complex known as the "RNA degradosome" can drive the energy-dependent turnover of mRNA and can trim some RNA species into their active forms (Carpousis *et al.*, 2002). The integral components of the RNA degradosome include the endoribonuclease RNase E (whose C-terminal part serves as a scaffold for the complex), the phosphorolytic exoribonuclease polynucleotide phosphorylase (PNPase), the DEAD-box RNA helicase RhlB, and enolase. RNase E initiates mRNA decay by cutting messages into fragments; the helicase RhlB facilitates the degradation of structured RNA by PNPase, which continues this degradation process in the 3'→5' direction.

While performing functional assays with RNA degradosomes assembled with mutant PNPases isolated in our laboratory (Briani *et al.* 2007), we observed that ATP concentrations higher than 5 mM retarded the appearance of degradation products. So this work was initially aimed at assessing whether ATP is actually capable of inhibiting the enzyme and at understanding mechanism and physiological role(s) of this effect.

Our results provide plenty of evidence confirming our hypothesis: in particular: i) ATP was inhibitory in a PNPase assay based on the detection of both elongation and degradation of a radiolabeled RNA probe, representative of synthetic and phosphorolytic activity, respectively ii) affinity labeling experiments by UV cross-linking radiolabeled ATP showed that the nucleotide actually binds the protein iii) kinetic assays based on photometric methods could detect PNPase inhibition in both the synthetic and the phosphorolytic direction.

Although this inhibitory effect is likely to play a major regulatory role, no such observation was reported to date despite over five decades of investigations on this enzyme. The ATP-binding site is distinct from that of the substrates, as substantiated by the mixed-type inhibition towards phosphate, and by the fact that no substrate could abolish or reduce the inhibitory effect even at saturating concentrations. As regards the inhibition pattern, replots of slopes and 1/v-axis intercepts as a function of inhibitor concentration did not yield straight lines as predicted by the classical mixed-type inhibition model. In contrast, the sigmoidal profile of PNPase inhibition as a function of ATP concentration indicates a cooperative, allosteric binding of the nucleotide. In particular, we assessed a Hill coefficient of 2.3, well in agreement with the trimeric structure of the enzyme, and a $I_{0.5}$ of 3.3 mM. Similar results were obtained at a poly(A) concentration close to the K_m, i.e. 2 μg/ml, and also using the whole

degradosome instead of PNPase alone. This latter observation implies that ATP may also modulate PNPase function at the level of the multi-protein complex. The nucleotide also exerted a comparable inhibition on the synthetic activity, with a Hill coefficient of 2.3 as in the phosphorolytic direction, and a $I_{0.5}$ of 5.0 mM. Our kinetic assays may not fully reproduce the physiological conditions, as ADP and phosphate are promptly removed by the auxiliary reactions in the phosphorolytic and synthetic tests, respectively. This, however, should not affect the mode of ATP inhibition, since the ATP-binding site is distinct from that of the substrates. Taken together, these results strongly support the idea that the inhibition exerted by ATP on PNPase is a phenomenon of physiological relevance. This is also substantiated by the fact that the inhibitory concentrations are in the range of the physiological values, namely 1-4 mM (Lasko and Wang 1996). Furthermore, enzymes displaying a sigmoidal dependence of their activity on metabolite concentrations are believed to exert major roles in metabolic regulation. However, the interpretation of our observations is not straightforward. Classical studies conducted by Atkinson several decades ago (Shen and Atkinson, 1970), established that high values of energy charge, and thus high ATP and low ADP and AMP, inhibit the catabolic pathways in both eukaryotes and prokaryotes. Unfortunately accurate assessment of the enzyme behavior under physiological conditions is not feasible as the local, intracellular concentration of phosphate and nucleotides can be hardly predicted. Nevertheless, our finding may help shed light on the physiological significance of different RNA degradation pathways operating in *E. coli*.

It has been pointed out that phosphorolytic degradation of mRNA by PNPase, which operates close to equilibrium, is more energy-saving than the hydrolysis performed by RNase II, which releases nucleoside

monophosphates and is far from equilibrium. Moreover, 3'-end tailing of RNA may be performed both by poly adenylate polymerase at the expenses of ATP and by PNPase, which uses NDPs. Thus PNPase-dependent degradation of RNA would be energetically more favorable than RNase II/PAP-dependent degradation and would be activated at a low energy charge. Additional regulatory levels might occur in the RNA degradosome and in the PNPase-RhlB complex, where the RNA helicase unwinds RNA secondary structures and hydrolyzes ATP. This could lower the local ATP concentration with concurrent PNPase activation. Conversely, a low helicase activity may allow a local increase of ATP concentration thus inhibiting RNA degradation. Predictions of the above speculations are that RNase II, the PNPase-RhlB complex and the RNA degradosome may perform RNA degradation at high energy charge, whereas free PNPase activity would be more relevant at low ATP concentrations.

In our further investigations we attempted to identify the ATP-binding sites by taking advantage of a modeling analysis. This led us to tentatively spot residues of two putative ATP-binding sites: Phe77, Phe78, Arg79 in one site; Phe56, Arg93, Phe103 in the other. We replaced by alanine each of these six residues, but in no case the inhibitory effect was abolished. This indicates that the modeling analysis failed to identify the nucleotide binding site. However, during these studies we also observed that the mutants R79A and F77A displayed reduced polymerization activity using ADP as a substrate, which suggests that the two mutated residues are involved in nucleotide substrate binding. However, only the mutant R79A displayed a substantially increased K_m for both ADP and phosphate, suggesting that Arg79 may be involved in both ADP and phosphate binding. Furthermore, the K_m for polyA of either mutants was comparable to that of the wt, which implies that they either are not involved in RNA binding, as suggested by Shi

et al. (2008) and by Nurmohamed *et al.* (2009), or that single mutations are not sufficient to cause a significant decrease in RNA binding.

References

Amblar, M., Arraiano, C. M. (2005) A single mutation in Escherichia coli ribonuclease II inactivates the enzyme without affecting RNA binding. *FEBS J.* 272: 363-374.

Amblar, M., Barbas, A., Fialho, A. M., and Arraiano, C. M. (2006). Characterization of the Functional Domains of Escherichia coli RNase II *J.Mol.Biol.* 360: 921-933.

Andrade, J. M., Cairrao, F., and Arraiano, C. M. (2006). RNase R affects gene expression in stationary phase: regulation of ompA *Mol.Microbiol.* **60**: 219-228.

Arnold, T. E., Yu, J., and Belasco, J. G. (1998) mRNA stabilization by the ompA 5' untranslated region: two protective elements hinder distinct pathways for mRNA degradation. *RNA.* 4: 319-330.

Arraiano, C. M. and Maquat, L. E. (2003) Post-transcriptional control of gene expression: effectors of mRNA decay. *Mol. Microbiol*. 49, 267–276.

Babitzke, P., Granger, L., Olszewski, J., and Kushner, S. R. (1993) Analysis of mRNA decay and rRNA processing in *Escherichia coli* multiple mutants carrying a deletion in RNase III. *J.Bacteriol.* 175: 229-239.

Babitzke, P., Kushner, S. R. (1991) The Ams (altered mRNA stability) protein and ribonuclease E are encoded by the same structural gene of *Escherichia coli. Proc.Natl.Acad.Sci.USA* 88: 1-5.

Bae, W., Xia, B., Inouye, M., and Severinov, K. (2000) *Escherichia coli* CspA-family RNA chaperones are transcription antiterminators. *Proc.Natl.Acad.Sci.U.S.A.* 97: 7784-7789.

Baker, K. E., Condon, C. (2004) Under the Tucson sun: a meeting in the desert on mRNA decay. *RNA.* 10: 1680-1691.

Belasco, J. G., Higgins, C. F. (1988) Mechanisms of mRNA decay in bacteria: a perspective. *Gene* 72: 15-23.

Belasco, J. G., Nilsson, G., von Gabain, A., and Cohen, S. N. (1986) The stability of *E. coli* gene transcripts is dependent on determinants localized to specific mRNA segments. *Cell* 46: 245-251.

Beran, R. K., Simons, R. W. (2001) Cold-temperature induction of *Escherichia coli* polynucleotide phosphorylase occurs by reversal of its autoregulation. *Mol.Microbiol.* 39: 112-125.

Berlyn, M. K. B. (1998) Linkage map of *Escherichia coli* K-12, Edition 10: the traditional map. *Microbiol.Mol.Biol.Rev.* 62: 814-984.

Bernstein, J.A., Lin, P. H., Cohen, S. N., Lin-Chao, S. (2004). Global analysis of Escherichia coli RNA degradosome function using DNA microarrays. *Proc. Natl. Acad. Sci. U. S. A*. 101, 2758–2763.

Bollenbach, T. J., Lange, H., Gutierrez, R., Erhardt, M., Stern, D. B., and Gagliardi, D. (2005) RNR1, a 3'-5' exoribonuclease belonging to the RNR superfamily, catalyzes 3' maturation of chloroplast ribosomal RNAs in Arabidopsis thaliana. *Nucleic Acids.Res.* 33: 2751-2763.

Boni, I. V., Isaeva, D. M., Musychenko, M. L. & Tzareva, N. V. (1991) Ribosome-messenger recognition: mRNA target sites for ribosomal protein S1. *Nucl. Acid Res.* 19, 155–162.

Briani, F., Del Favero, M., Capizzuto, R., Consonni, C., Zangrossi, S., Greco, C., De Gioia, L., Tortora, P., Dehò, G. (2007) Genetic analysis of polynucleotide phosphorylase structure and functions. *Biochimie*. 89: 145-157

Briani, F., Del Vecchio, E., Migliorini, D., Hajnsdorf, E., Regnier, P., Ghisotti, D., Dehò, G. (2002) RNase E and polyadenyl polymerase I are involved in maturation of CI RNA, the P4 phage immunity factor. J. *Mol. Biol*. 318, 321-31.

Briegel, K. J., Baker, A., Jain, C. (2005) Identification and analysis of *Escherichia col*i ribonuclease E dominant-negative mutants. *Genetics* 172, 7–15.

Buttner, K., Wenig, K., and Hopfner, K.-P. (2005) Structural frame work for the mechanism of archaeal exosomes in RNA processing. *Mol. Cell* 20: 461–471.

Bycroft, M., Hubbard, T. J., Proctor, M., Freund, S. M., and Murzin, A. G. (1997) The solution structure of the S1 RNA binding domain: a member of an ancient nucleic acid-binding fold. *Cell* 88: 235-242.

Cairrão, F. and Arraiano, C. M. (2006) The role of endoribonucleases in the regulation of RNase R. *Biochem. Biophys. Res. Comm*. 343, 731–737.

Cairrão, F., Chora, A., Zilhão, R., Carpousis, J. and Arraiano, C. M. (2001) RNase II levels change according to the growth conditions: characterization of gmr, a new Escherichia coli gene involved in the modulation of RNase II. *Mol. Microbiol*. 276, 19172–19181.

Callaghan, A. J., Aurikko, J. P., Ilag, L. L., Gunter, G. J., Chandran, V., Kuhnel, K., Poljak, L., Carpousis, A. J., Robinson, C. V., Symmons, M. F., and Luisi, B. F. (2004) Studies of the RNA degradosome-organizing domain of the Escherichia coli ribonuclease RNase. E *J.Mol.Biol.* 340: 965-979.

Callaghan, A. J., Grossmann, J. G., Redko, Y. U., Ilag, L. L., Moncrieffe, M. C., Symmons, M. F., Robinson, C. V., McDowall, K. J., Luisi, B. F. (2003) Quaternary structure and catalytic activity of the Escherichia coli ribonuclease E amino-terminal catalytic domain. *Biochemistry* 42, 13848–13855.

Callaghan, A. J., Marcaida, M. J., Stead, J. A., McDowall, K. J., Scott, W. G., and Luisi, B. F. (2005) Structure of Escherichia coli RNase E catalytic domain and implications for RNA turnover. *Nature* 437: 1187-1191.

Carpousis, A. J. (2003) Degradation of targeted mRNAs in Escherichia coli: regulation by a small antisense RNA. *Genes Dev.* 17: 2351-2355.

Carpousis, A. J., Van Houwe, G., Ehretsmann, C., and Krisch, H. M. (1994) Copurification of *E. coli* RNase E and PNPase: evidence for a specific association between two enzymes important in RNA processing and degradation. *Cell* 76: 889-900.

Carpousis, A. J., Vanzo, N. F., and Raynal, L. C. (1999) mRNA degradation. A tale of poly(A) and multiprotein machines. *Trends Genet.* 15: 24-28.

Caruthers, J. M., and McKay, D. B. (2002) Helicase structure and mechanism. *Curr. Opin. Struct. Biol.* 12, 123-133.

Celesnik, H., Deana, A., and Belasco, J. G. (2007) Initiation of RNA decay in Escherichia coli by 5' pyrophosphate removal. *Mol.Cell* 27: 79-90.

Chandran, V. and Luisi, B.F. (2006) Recognition of enolase in the *Escherichia coli* RNA degradosome. *J. Mol. Biol*. 358, 8–15.

Charollais, J., Pflieger, D., Vinh, J., Dreyfus, M., and Iost, I. (2003) The DEAD-box RNA helicase SrmB is involved in the assembly of 50S ribosomal subunits in Escherichia coli. *Mol. Microbiol.* 48, 1253-1265.

Chen, C. Y., Beatty, J. T., Cohen, S. N., and Belasco, J. G. (1988) An intercistronic stem-loop structure functions as an mRNA decay terminator necessary but insufficient for puf mRNA stability. *Cell* 52: 609-619.

Cheng, Z.-F., Zuo, Y., Li, Z., Rudd, K. E. and Deutcher, M. P. (1998). The vacB gene required for virulence in *Shigella flexeneri* and *Escherichia coli* encodes the exoribonuclease RNase R*. J. Biol. Chem*. 273, 14077–14080.

Coburn, G. A., Mackie, G. A. (1999) Degradation of mRNA in *Escherichia coli*: an old problem with some new twists. *Prog.Nucleic Acid.Res.Mol.Biol.* 62: 55-108.

Cohen, S. N., McDowall, K. J. (1997) RNase E: still a wonderfully mysterious enzyme. *Mol.Microbiol.* 23: 1099-1106.

Condon,C. (2007) Maturation and degradation of RNA in bacteria. *Curr.Opin.Microbiol.* 10: 271-278.

Datsenko, K. A., Wanner, B. L. (2000) One-step inactivation of chromosomal genes in *Escherichia coli* K-12 using PCR products. *Proc. Natl. Acad. Sci. USA* 97, 6640-45.

Deana, A. and Belasco, J. G. (2004) The function of RNase G in Escherichia coli is constrained by its amino and carboxyl termini. *Mol. Microbiol.* 51, 1205–1217.

Deana, A., Celesnik, H., and Belasco, J. G. (2008) The bacterial enzyme RppH triggers messenger RNA degradation by 5' pyrophosphate removal. *Nature* 451: 355-358.

Deutcher, M. P. (2006) Degradation of RNA in bacteria: comparison of mRNA and stable RNA. *Nucl. Acids Res*. 34, 659-666

Deutscher, M. P., Li, Z. (2001) Exoribonucleases and their multiple roles in RNA metabolism. *Prog.Nucleic Acid.Res.Mol.Biol.* 66: 67-105.

Deutscher, M. P., Reuven, N. B. (1991) Enzymatic basis for hydrolytic versus phosphorolytic mRNA degradation in *Escherichia coli* and *Bacillus subtilis. Proc.Natl.Acad.Sci.USA* 88: 3277-3280.

Ghora, B. K., Apirion, D. (1978) Structural analysis and in vitro processing to p5 rRNA of a 9S RNA molecule isolated from an rne mutant of *E. coli*. *Cell* 15: 1055-1066.

Ghosh, S., Deutscher, M. P. (1999) Oligoribonuclease is an essential component of the mRNA decay pathway. *Proc.Natl.Acad.Sci.USA* 96: 4372-4377.

Goodford, P. J. (1985) A Computational-procedure for determining energetically favorable binding sites on biologically important macromolecules. *J.Med.Chem.* 28: 849-857

Graumann P.L., and Marahiel M.A. (1998) A superfamily of proteins that contain the cold-shock domain. *Trends Biochem Sci* 23, 286-290.

Grunberg-Manago, M. (1999) Messenger RNA stability and its role in control of gene expression in bacteria and phages. *Annu.Rev.Genet.* 33: 193-227.

Grunberg-Manago, M., Ortiz, P. J., and Ochoa, S. (1955) Enzymatic synthesis of nucleic acidlike polynucleotides. *Science* 122: 907-910.

Gualerzi, C. O., Giuliodori, A. M., and Pon, C. L. (2003) Transcriptional and post-transcriptional control of cold-shock genes. *J.Mol.Biol.* 331: 527-539.

Huttenhofer, A., Noller, H. F. (1994) Footprinting mRNA-ribosome complexes with chemical probes. *EMBO J.* 13: 3892-3901.

Iost, I., Dreyfus, M. (1995) The stability of Escherichia coli lacZ mRNA depends upon the simultaneity of its synthesis and translation. *EMBO J.* 14: 3252-3261.

Jarrige, A. C., Mathy, N., and Portier, C. (2001) PNPase autocontrols its expression by degrading a double-stranded structure in the *pnp* mRNA leader. *EMBO J.* 20: 6845-6855.

Jarrige, A., Bréchemier-Baey, D., Mathy, N., Duche, O., and Portier, C. (2002) Mutational analysis of polynucleotide phosphorylase from *Escherichia coli. J.Mol.Biol.* 321: 397-409.

Jiang, X., Diwa, A., and Belasco, J. G. (2000) Regions of RNase E important for 5'-end-dependent RNA cleavage and autoregulated synthesis. *J.Bacteriol.* 182: 2468-2475.

Jones, P. G., Mitta, M., Kim, Y., Jiang, W., and Inouye, M. (1996) Cold shock induces a major ribosomal-associated protein that unwinds double-stranded RNA in *Escherichia coli. Proc.Natl.Acad.Sci.U.S.A* 93: 76-80.

Kalman, M., Murphy, H., and Cashel, M. (1991) rhlB, a new Escherichia coli K-12 gene with an RNA helicase-like protein sequence motif, one of at least five such possible genes in a prokaryote. *New Biol.* 3: 886-895.

Kawamoto, H., Morita, T., Shimizu, A., Inada, T., and Aiba, H. (2005) Implication of membrane localization of target mRNA in the action of a small RNA: mechanism of post-transcriptional regulation of glucose transporter in Escherichia coli. G*enes Dev.* 19: 328-338.

Khemici, V., Carpousis, A. J. (2004) The RNA degradosome and poly(A) polymerase of *Escherichia coli* are required in vivo for the degradation of small mRNA decay intermediates containing REP-stabilizers. *Mol.Microbiol.* 51: 777-790.

Khemici, V., Poljak, L., Toesca, I., and Carpousis, A. (2005) Evidence *in vivo* that the DEAD-box RNA helicase RhlB facilitates the degradation of ribosome-free mRNA by RNase E*. PNAS* 102, 6913-6918.

Khemici, V., Toesca, I., Poljak, L., Vanzo, N. F., and Carpousis, A. J. (2004) The RNase E of *Escherichia coli* has at least two binding sites for DEAD-box RNA helicases: functional replacement of RhlB by RhlE. *Mol Microbiol* 54: 1422-1430.

Kuhnel K, Luisi B. F. (2001) Crystal structure of the Escherichia coli RNA degradosome component enolase. *J.Mol.Biol.* 313: 583-592

Lee, K., Bernstein, J. A., and Cohen, S. N. (2002) RNase G complementation of rne null mutation identifies functional interrelationships with RNase E in *Escherichia coli*. *Mol.Microbiol.* 43: 1445-1456.

Leroy, A., Vanzo, N. F., Sousa, S., Dreyfus, M., and Carpousis, A. J. (2002) Function in *Escherichia coli* of the non catalytic part of RNase E: role in the degradation of ribosome-free mRNA. *Mol microbiology* 45, 1231-1243.

Leszczyniecka, M., DeSalle, R., Kang, D. C., and Fisher, P. B. (2004) The origin of polynucleotide phosphorylase domains. *Mol Phylogenet.Evol.* 31: 123-130.

Li, Z., and Deutscher, M.P. (2002) RNase E plays an essential role in the maturation of *Escherichia coli* tRNA precursors. *RNA* 8, 97–109.

Li, Z., Pandit, S., and Deutscher, M. P. (1999) RNase G (Caf A protein) and RNase E are both required for the 5' maturation of 16S ribosomal RNA. *EMBO J* 18, 2878-2885.

Lim, J., Kuroki, T., Ozaki, K., Kohsaki, H., Yamori, T., Tsuruo, T., Nakamori, S., Imaoka, S., Endo, M., and Nakamura,Y. (1997) Isolation of murine and human homologues of the fission-yeast dis3+ gene encoding a mitotic-control protein and its overexpression in cancer cells with progressive phenotype. *Cancer Res.* 57: 921-925.

Littauer, U. Z. and Kornberg, A (1957) Reversible synthesis of polyribonucleotides with an enzyme from Escherichia coli. *J Biol Chem*. 226, 1077-1092

Lopez, P., Marchand, I., Joyce, S. A., and Dreyfus, M. (1999) The C-terminal half of RNase E, which organizes the Escherichia coli degradosome, participates in mRNA degradation but not rRNA processing in vivo *Mol. Microbiol*. 33, 188-199.

Lorentzen, E., Walter, P., Fribourg, S., Evguenieva-Hackenberg, E., Klug, G., and Conti, E. (2005). The archaeal exosome core is a hexameric ring structure with three catalytic subunits. *Nat. Struct. Mol. Biol*. 12: 575–581.

Luttinger, A., Hahn, J., and Dubnau, D. (1996) Polynucleotide phosphorylase is necessary for competence development in *Bacillus subtilis. Mol.Microbiol.* 19: 343-356.

Majdalani, N., Vanderpool, C., and Gottesman, S. (2005) Bacterial small RNA regulators. *Crit.Rev.Biochem.Mol.Biol.* 40: 93-113.

Marcaida, M. J., Depristo, M. A., Chandran, V., Carpousis, A. J., and Luisi, B. F. (2006) The RNA degradosome: life in the fast lane of adaptive molecular evolution. *Trends Biochem.Sci.*

Masse, E., Majdalani, N., and Gottesman, S. (2003) Regulatory roles for small RNAs in bacteria. *Curr.Opin.Microbiol.* 6: 120-124.

Matus-Ortega, M. E., Regonesi, M. E., Pina-Escobedo, A., Tortora, P., Dehò, G., and Garcia-Mena, J. (2007) The KH and S1 domains of Escherichia coli

polynucleotide phosphorylase are necessary for autoregulation and growth at low temperature. *Biochim. Biophys. Acta*. 1769, 194-203.

McDowall, K. J., Cohen, S. N. (1996) The N-terminal domain of the rne gene product has RNase E activity and is non-overlapping with the arginine-rich RNA-binding site. *J.Mol.Biol.* 255: 349-355.

McDowall, K. J., Hernandez, R. G., Lin-Chao, S., and Cohen, S. N. (1993) The ams-1 and rne-3071 temperature-sensitive mutations in the ams gene are in close proximity to each other and cause substitutions within a domain that resembles a product of the Escherichia coli mre locus. *J.Bacteriol.* 175: 4245-4249.

McDowall, K. J., Lin-Chao, S., and Cohen, S. N. (1994) A+U content rather than a particular nucleotide order determines the specificity of RNase E cleavage. *J.Biol.Chem.* 269: 10790-10796.

Melefors, Ö., and von Gabain, A. (1991) Genetic studies of cleavage-initiated mRNA decay and processing of ribosomal 9S RNA show that the *Escherichia coli ams* and *rne* loci are the same. *Mol Microbiol* 5, 57–864.

Mian, I. S. (1997) Comparative sequence analysis of ribonucleases HII, III, II PH and D. *Nucleic Acids.Res.* 25: 3187-3195.

Mohanty, B. K., Kushner, S. R. (2000) Polynucleotide phosphorylase functions both as a 3' right-arrow 5' exonuclease and a poly(A) polymerase in *Escherichia coli. Proc.Natl.Acad.Sci.U.S.A* 97: 11966-11971.

Morita, T., Kawamoto, H., Mizota, T., Inada, T., and Aiba, H. (2004) Enolase in the RNA degradosome plays a crucial role in the rapid decay of glucose transporter mRNA in the response to phosphosugar stress in *Escherichia coli. Mol Microbiol* 54: 1063-1075.

Morita, T., Maki, K., and Aiba, H. (2005) RNase E-based ribonucleoprotein complexes: mechanical basis of mRNA destabilization mediated by bacterial noncoding RNAs. *Genes Dev.* 19: 2176-2186.

Mott, J. E., Galloway, J. L., and Platt, T. (1985) Maturation of Escherichia coli tryptophan operon mRNA: evidence for 3' exonucleolytic processing after rho-dependent termination. *EMBO J.* 4: 1887-1891.

Mudd, E. A., Carpousis, A. J., and Krisch, H. M. (1990) *Escherichia coli* RNase E has a role in the decay of bacteriophage T4 mRNA. *Genes Dev.* 4: 873-881.

Nishi, K., Morel-Deville, F., Hershey, J. W., Leighton, T., and Schneir, J. (1988) An EIF-4A-like protein is a suppressor of an *Escherichia coli* mutant defective in 50s ribosomal subunit assembly. *Nature* 336, 496-498.

Noguchi, E., Hayashi, N., Azuma, Y., Seki, T., Nakamura, M., Nakashima, N., Yanagida, M., He, X., Mueller, U., Sazer, S., and Nishimoto, T. (1996) Dis3, implicated in mitotic control, binds directly to Ran and enhances the GEF activity of RCC1. *EMBO J.* 15: 5595-5605.

Nurmohamed, S., Vaidialingam, B., Callaghan, A. J., and Luisi, B. F. (2009) Crystal structure of *Escherichia coli* Polynucleotide Phosphorylase core bound to RNase E, RNA and manganese: implications for catalytic mechanism and RNA degradosome assembly. *J.Mol.Biol.* 389: 17-23.

Okada, Y., Wachi, M., Hirata, A., Suzuki, K., Nagai, K., and Matsuhashi, M. (1994) Cytoplasmic axial filaments in Escherichia coli cells: possible function in the mechanism of chromosome segregation and cell division. *J.Bacteriol.* 176: 917-922.

Ono, M., Kuwano, M. (1979) A conditional lethal mutation in an Escherichia coli strain with a longer chemical lifetime of messenger RNA. *J.Mol.Biol.* 129: 343-357.

Ow, M. C. and Kushner, S. R. (2002) Initiation of tRNA maturation by RNase E is essential for cell viability in *Escherichia. coli. Genes Dev.* 16, 1102–1115.

Ow, M. C., Kushner, S. R. (2002) Initiation of tRNA maturation by RNase E is essential for cell viability in *E. coli. Genes Dev.* 16: 1102-1115.

Ow, M. C., Liu, Q., and Kushner, S. R. (2000) Analysis of mRNA decay and rRNA processing in *Escherichia coli* in the absence of RNase E-based degradosome assembly. *Mol.Microbiol.* 38: 854-866.

Petersen, C. (1991) Multiple determinants of functional mRNA stability: sequence alterations at either end of the lacZ gene affect the rate of mRNA inactivation. *J.Bacteriol.* 173: 2167-2172.

Piazza, F., Zappone, M., Sana, M., Briani, F., and Deho, G. (1996) Polynucleotide phosphorylase of Escherichia coli is required for the establishment of bacteriophage P4 immunity. *J.Bacteriol.* 178: 5513-5521.

Portier, C., Dondon, L., Grunberg-Manago, M., and Régnier, P. (1987) The first step in the functional inactivation of the *Escherichia coli* polynucleotide phosphorylase messenger is a ribonuclease III processing at the 5' end. *EMBO J.* 6: 2165-2170.

Portier, C., Régnier, P. (1984) Expression of the *rpsO* and *pnp* genes: structural analysis of a DNA fragment carrying their control regions. *Nucleic Acids.Res.* 12: 6091-6102.

Py, B., Causton, H., Mudd, E. A., and Higgins, C. F. (1994) A protein complex mediating mRNA degradation in *Escherichia coli. Mol.Microbiol.* 14: 717-729.

Py, B., Higgins, C. F., Krisch, H. M., and Carpousis, A. J. (1996) A DEAD-box RNA helicase in the *Escherichia coli* RNA degradosome. *Nature* 381: 169-172.

Py, B., Higgins, C.F., Krisch, H. M., and Carpousis, A. J. (1996) A DEAD-box RNA helicase in the *Escherichia coli* RNA degradosome. *Nature* 381, 169-172.

Ray, B. K., and Apirion, D. (1981) RNAase P is dependent on RNAase E action in processing monomeric RNA precursors that accumulate in an RNAase E-mutant of *Escherichia coli*. *J Mol Biol* 149, 599–617.

Régnier, P., Grunberg-Manago, M. (1990) RNase III cleavages in non-coding leaders of *Escherichia coli* transcripts control mRNA stability and genetic expression. *Biochimie* 72: 825-834.

Regonesi, M. E., Briani, F., Ghetta, A., Zangrossi, S., Ghisotti, D., Tortora, P., and Deho, G. (2004) A mutation in polynucleotide phosphorylase from Escherichia coli impairing RNA binding and degradosome stability. *Nucleic Acids Res.* 32: 1006-1017.

Regonesi, M. E., Del Favero, M., Basilico, F., Briani, F., Benazzi, L., Tortora, P., Mauri, P., and Deho, G. (2006) Analysis of the Escherichia coli RNA degradosome composition by a proteomic approach. *Biochimie* 88: 151-161.

Robert-Le Meur, M., Portier, C. (1992) E.coli polynucleotide phosphorylase expression is autoregulated through an RNase III-dependent mechanism. *EMBO J.* 11: 2633-2641.

Robert-Le Meur, M., Portier, C. (1994) Polynucleotide phosphorylase of *Escherichia coli* induces the degradation of its RNase III processed messenger by preventing its translation. *Nucleic Acids.Res.* 22: 397-403.

Rogers, G. W., Jr, Komar, A. A., and Merrick., W. C. (2002) ElF4A: The godfather of the DEAD box helicases. *Prog. Nucleic. Acid. Res. Mol. Biol*. 72, 307-331.

Segel, I. H. (1975) *Enzyme Kinetics,* John Wiley & Sons, Inc., New York.

Sharp,J.S., Bechhofer,D.H. (2003) Effect of translational signals on mRNA decay in Bacillus subtilis *J.Bacteriol.* 185: 5372-5379.

Shen, L. C., and Atkinson, D. E. (1970) Regulation of pyruvate dehydrogenase from Escherichia coli. Interactions of adenylate energy charge and other regulatory parameters. *J. Biol. Chem.* 245, 5974–5978.

Shi, Z., Yang, W. Z., Lin-Chao, S., Chak, K. F., and Yuan, H. S. (2008) Crystal structure of *Escherichia coli* PNPase: central channel residues are involved in processive RNA degradation. *RNA*. 14: 2361-2371.

Silverman, E., Edwalds-Gilbert, G. and Lin, R. J. (2003) DExD/H-box proteins and their partners: helping RNA helicases unwind. *Gene* 312, 1-16.

Spickler, C., Mackie, G. A. (2000) Action of RNase II and polynucleotide phosphorylase against RNAs containing stem-loops of defined structure. *J.Bacteriol.* 182: 2422-2427.

Stickney, L. M., Hankins, J. S., Miao, X., and Mackie, G. A. (2005) Function of the Conserved S1 and KH Domains in Polynucleotide. Phosphorylase *J.Bacteriol.* 187: 7214-7221.

Symmons M.F., Williams M.G., Luisi B.F., Jones G.H., and Carpousis A.J. (2002) Running rings around RNA: a superfamily of phosphate-dependent RNases. *Trends in Biochemical Sciences* 27, N° 11-18.

Symmons, M. F., Jones, G. H., and Luisi, B. F. (2000) A duplicated fold is the structural basis for polynucleotide phosphorylase catalytic activity, processivity, and regulation. *Structure Fold.Des.* 8: 1215-1226.

Tanner, N. K. and Linder, P. (2001) DExD/H box RNA helicases: From generic motors to specific dissociation functions. *Mol. Cell.* 8, 251-262.

Taraseviciene, L., Miczak, A., and Apirion, D. (1991) The gene specifying RNase E (*rne*) and a gene affecting mRNA stability (ams) are the same gene. *Mol Microbiol* 5, 851– 855.

Tock, M. R., Walsh, A. P., Carroll, G., and McDowall, K. J. (2000) The CafA protein required for the 5'-maturation of 16 S rRNA is a 5'-end-dependent ribonuclease that has context-dependent broad sequence specificity. *J.Biol.Chem.* 275: 8726-8732.

Van Hoof, A., Lennertz, P., and Parker, R. (2000) Three conserved members of the RNase D family have unique and overlapping functions in the processing of 5S, 5.8S, U4, U5, rnASE MRP and RNase P RNAs in yeast. *EMBO J.* 19, 1357-1365.

Vanzo N. F., Li Y. S., Py B., Blum E., Higgins C. F., Raynal L. C., Krisch H. M., and Carpousis A. J. (1998) Ribonuclease E organizes the protein interactions in the *Escherichia coli* RNA degradosome. *Genes Dev* 12, 2770-2781.

Viegas, S. C., Schmidt, D., Kasche, V., Arraiano, C. M. & Ignatova, Z. (2005) Effect of the increased stability of the penicillin amidase mRNA on the protein expression levels. *FEBS Letters* 579, 5069–5073.

Wachi, M (1999). *Escherichia coli cafA* gene encodes a novel RNase, designated as RNase G, involved in processing of the 50 end of 16S rRNA. Biochem. Biophys. *Res. Commun*. 259, 483–488.

Wachi, M., Umitsuki, G., and Nagai, K. (1997) Functional relationship between Escherichia coli RNase E and the CafA protein. *Mol.Gen.Genet.* 253: 515-519.

Wagner, E. G., Simons, R. W. (1994) Antisense RNA control in bacteria, phages, and plasmids. *Annu.Rev.Microbiol.* 48: 713-742.

Webb, M. R. (1992) A continuos spectrophotometric assay for inorganic phosphate and for measuring hosphate release kinetics in biological systems. *Proc. Natl. Acad. Sci. U.S.A.* 89: 4884-488

Worrall, J. A., Luisi, B. F. (2007) Information available at cut rates: structure and mechanism of ribonucleases. *Curr.Opin.Struct.Biol.* 17: 128-137.

Zangrossi, S., Briani, F., Ghisotti, D., Regonesi, M. E., Tortora, P., and Deho, G. (2000) Transcriptional and post-transcriptional control of polynucleotide phosphorylase during cold acclimation in Escherichia coli. *Mol.Microbiol.* 36: 1470-1480.

Zilhao, R., Cairrao, F., Régnier, P., and Arraiano, C. M. (1996) PNPase modulates RNase II expression in Escherichia coli: implications for mRNA decay and cell metabolism. *Mol.Microbiol.* 20: 1033-1042.

Zuo, Y., and Deutscher, M. P. (2001) Survey and Summary. Exoribonuclease superfamilies: structural analysis and phylogenetic distribution. *Nucl. Acids Res*. 209, 1017–1026.